Applied Electromagnetism
Mekelweg 4,
2628 CD Delft
The Netherlands
http://ens.ewi.tudelft.nl/

THS-2012-4117719

M.Sc. Thesis

Ultra -Wideband Leaky- Wave Antenna for Medical Imaging

Kalyan Vaddagiri

Faculty of Electrical Engineering, Mathematics and Computer Science **Delft University of Technology**

Abstract

Cancer can be viewed as a curse on life of any man or woman. Although some tumors that are malignant can be curable, it comes at a cost of unbearable pain and mental trauma. X-ray based techniques are being used for many decades for detecting tumors. These techniques are applied at the expense of exposure to high ionized radiation levels. Magnetic Resonance Imaging (MRI) is another technique which is a noninvasive medical diagnosis for detecting tumors. However, MRI is quite expensive test and the powerful magnetic field of the MRI system may damage an external hearing aid or cause a heart pacemaker or electrical stimulator, or neuro stimulator to malfunction.

In recent times, the rapid advancement in radar and microwave technology has attracted the attention of the biomedical engineering community for application to medical imaging. The capability for penetrating waves into human body, non ionizing radiation and possibility of high resolution through UWB technology makes microwave technology an attractive alternative in biomedical imaging.

In this thesis, first a comparative study of UWB antennas proposed in the open literature for imaging is performed. This study outline some of the most significant intrinsic limitations of these antennas. Next taking into account a wide range of technical and medical concerns, this thesis addresses the analysis and designing of a novel antenna for imaging tumors inside the human body in the frequency region of $3 - 10$ GHz. Thus, we propose an effective design strategy that combines theoretical inputs, and technological constraints to design the novel leaky slot antenna. We believe that our results pave the way for future research oriented to the design of a complete microwave imaging medical system for medical application.

Keywords : Dielectric constant, Fidelity Factor, Matching Medium, Leaky- Wave phenemenon, Phase Center, UWB.

Acknowledgments

I would like to thank my guru Dr.Prof.Andrea Neto for showing me different aspects in antenna technology. Andrea's dedication to work, humor and criticism on the developed antennas has an impact in my career life and i am always indebted to my guru in this aspect. You are a role model for me, and the amount of useful advice you provided to me is uncountable. The joy and the enthusiasm you have, for the research of "novel antennas" is contagious and motivational for anyone. Without your help during these 9 months the results we achieved would not be possible and the dream to see leaky array in commerical market for detecting tumors inside human body would be left as dream. Grazie mille professore.

I am also grateful to my TNO supervisor Dr.ir.Stefania Monni for her patience and for her constant support during these 9 months. She always had time to clear my doubts and listen to my queries to help me out in solving the problems. I shall never forget the tips you gave me in my life. Thanks for believing me and for introducing me to many professors whenever you encountered. Thanks for the trust you had in me for doing a PHD . Irrespective of problems you had encountered, you always had time for me to help me out in this thesis. Grazie stefania.

I am thankful to Dr.ing. I.E. Lager for reviewing my thesis and providing me technical tips and hitches in the antenna development. I would also like to thank Dr.ir. Rob Remis for accepting to participate in my thesis defense.

I am grateful to Dr.ir.Daniele Cavallo for his patience in teaching basic antenna concepts and creative sketches. Your witty jokes and imitation on everyone are unlimited and your always ready to help attitude is not matchable with anyone. Thanks for helping me to understand about the difference between a monopole and a novel antenna. I thank you from my bottom of the heart for being such a good friend in/outside the professional environment. There are many good things about you but pages are limited. Grazie Cavallo.

Thanks to my colleague Dr.ir Annalisa for sharing many ideas and concepts in the field of antennas. Your help during thesis writing is appreciated.

A special thanks to Dr.ir.Wim van Rossum and ir. Daniela Deiana for making me to understand about antenna in terms of signal processing architecture.

A very special thanks to Frans Nennie for his daily help and for his enthusiasm in this project to develop the product prototype. You are more like a family member Frans. Apart from this, special thanks to Laura, Lorenzo, Roland, Fransceso and everyone in the Antenna and Radar group who made my 9 months thesis memorable.

Special thanks to Waqas for being like a friend, like a brother and for encouraging me to join this group. I shall remember you for the geekiness you exhibited during ESOA course in croatia. I have never seen a guy who wakes up in the night and talks about a waveguide

port and also for the swimming adventure you did in the croatia.

Dr.Nurhan and Dr.Fikret (beautiful couple from TURKEY) and Ozan you guys are more than group members. Hope my weekly presentations wouldn't have bored you and thanks for being friendly during this journey in this lab.

Iam thankful to my KuchBhi friends who stood beside me during last year and for the wonderful parties we had during the whole last year. Special thanks to my friends Venkat,Prasanna, Anto , Praveen and Venugopal Prasanth who stood beside me during exam times and for facing the odd together in these 2 years. Thanks to u guys for making these 2 years such a wonderful one.

Also special thanks to Ershad Ahmed for helping me out with latex problems. At any point of time you were always there to help me out in many issues. Thanks a lot buddy.

Last but not least to my mom who stood beside me for every up and down during these two year period and to my father who never hesitated to spend money on me for watever i ask for. I will forever be indebted and grateful to you for your sacrifices and examples that encouraged me to seek a higher education and to pursue a life-long goal of learning. You have also put up with me going away for 3 years, while always supporting me through this period.

I dedicate my thesis to my Lord Saibaba.

Kalyan Vaddagiri
Delft, The Netherlands
28-June -2012

Contents

List of Figures

List of Tables

1 Introduction

In the 1970s, Larsen and Jacobi carried out extensive experiments using microwave radiation to image canine kidneys[7]. They were successful in producing two-dimensional (2-D) images where various tissues were clearly discernible which triggered the attention of the microwave community. From then many research institutes and researchers started to develop tools for the early stage detection of tumor inside the human body. Although many researchers claimed early detection of tumors is possible, the statistics show that almost 3200 female deaths has been registered in Netherlands for breast cancer in the year 2010[8]. Estimated deaths for breast cancer in the United States in 2012 : 39,510 (female); 410 (male) [9]. From this, it derives the need for the advancement in technology in detecting cancer in early stage.

1.1 Motivation

For more than two decades X - ray and Magnetic Resonance Imaging (MRI) techniques have been used to detect tumors inside the human body[10]. These imaging methods provide diagnostic and critical information in respect to size and location of the tumor. Limitations of these methods are due to usage of ionizing radiation (X-ray) and relatively high costs (MRI) and the fact that the effectiveness of these methods are often limited to specific cases. During the procedure in X- ray, the area of interest is compressed and hold still by a dedicated machine to enhance the image quality which causes patient to undergo severe pain and inconvenience. In case of MRI , patient cannot undergo scanning if she has already an inbuilt electrical device.

X-ray mammography has a false-positive rate between 2.8% - 15.9% and a false-negative (missed cancer) rate between 4% - 34% [11]. The false-positive rate is due to the pursuit of the highest sensitivity or because of emotional strains inside the human body tissue. Concerning the false-negative rate, it is partially due to the observer error, but more frequently it is because the malignant tumor is hidden by other dense tissue. Moreover, another drawback of frequent testing with X - ray mammography could lead to cancer in younger females due to the increased ionized radiation [12].

The false-positive rate of MRI has been a concern by many clinicians. As criteria are refined and experience is gained, the specificity of breast MRI has increased significantly over the past several years. The false-positive rate is highly variable between studies, with many as low as 4 to 5 percent and others measuring 13 to 14 % [13].

1.2 Introduction to Microwave Imaging

The dielectric properties of human body tissue at microwave frequencies are sensitive to physiological factors of clinical interest, including water content, temperature, and

vascularization [14]. The studies conducted by Chaudary et al [14] , Joines et al [15] on the dielectric properties of healthy and cancerous tissues at microwave frequencies revealed that dielectric constant and conductivity for cancerous tissue are three or four times greater than that of normal tissue. Accordingly, there has been much recent interest in developing and applying microwave imaging techniques for the purpose of detecting and diagnosing tumor detection inside human body [16].

Active microwave imaging (MWI) of the human body involves transmitting low-power nonionizing narrowband or wideband microwave signals into the area of interest using an antenna array, which in turn measures the scattered microwave signals. For this purpose, two active types of microwave imaging techniques - tomography and radar based are being used to measure the scattered microwave signals.

Microwave tomography is based on diffraction based imaging. The dielectric properties are reconstructed back from the measurements based on the signals transmitted through UWB antennas into the human body. Reconstruction of images is based on iterative model procedures which are computationally extensive, as they always try to minimize the errors between measured and calculated electric fields.

In contrast to microwave tomography, radar based approach does not involve complex and computer intensive procedures. Radar based approach tries to identify the difference in the permittivity due to scattering of small objects such as tumors. The scattered signals are processed to generate a map of backscattered microwave energy based on simple sum and delay algorithm approach. Both the methods have advantages and disadvantages, but radar based approaches overcomes the computational challenges of conventional microwave tomography and permits full three dimensional imaging.

In this thesis frame work we chose UWB radar based technique which appears most relevant approach .The reason to choose the frequency region 3 -10 GHz is the trade off between higher resolution and depth of penetration. The requirement for penetration of tissues is satisfied with a low frequency of operation; in contrast, for an enhanced resolution, higher operation frequencies would fulfill the demand.

1.3 Problem Definition

To the best of knowledge, microwave based radar imaging research started in 1998. Until now only few prototypes have reached the stage of clinical experimentation [17] [18]. One of the reasons is that antennas currently used do not allow to achieve the required performance for the overall radar system.

In UWB region the phase center stability is a critical aspect especially when the signals transmitted and received are characterized by an UWB spectrum. In absence of phase center stability, compensation techniques resorting heavily to digital signal processing have to be used. A way to achieve phase center stability is by resistive loading of the antennas. In this case the antenna can be realized with dimension that are very small in terms of the wavelength (thus with no phase center uncertainty), while suppressing resonant behaviors.

This solution comes at the expense of low radiation efficiency which directly impacts the dynamic range of the radar system and signal to noise ratio.

Taking into account wide range of technical and medical concerns, this master thesis addresses the analysis, design, realization and characterization of a novel leaky slot antenna for medical imaging. It is a multidisciplinary topic which involves aspects of Electromagnetics (EM) wave interaction with biological tissue and field propagation in lossy matter.

1.4 Research Objectives

→ Analyze the influence of noise temperature in the system level design.

→ Link budget analysis.

→ Analyze the exisiting UWB antennas and their properties.

→ Design a new novel antenna for analyzing tumors inside human body.

→ Investigate safety issues such as tissue heating.

1.5 Constraints on the Use of UWB Technology

The interest in the Ultra - Wide Band (UWB) frequency region is due to commercial availability of components operating in such band leading to a renewed interest in developing UWB antennas. In 2002 the Federal Communications Commission (FCC) released first regulatory resolution allowing UWB transmissions under an unlicensed regime and later in 2007 the European Community (ECC) released UWB mask between the frequency region $3 - 10$ GHz. Various categories of applications have been classified by FCC with different regulations in each case which can be observed in Table 1.1

Applications	Frequency of operation	User limitations
Communications	3.1 to 10.6 GHz	No
Imaging:Ground penetrating radar, Medical imaging	960 MHz or 3.1 to 10.6 GHz	Yes
Imaging : Surveillance	1.99 to 10.6 GHz	Yes
Vehicular	24 to 29 GHz	No

Table 1.1: Approved FCC applications [4]

1.6 Maximum Permissible Energy Exposure

In 2007 the European commission committee (ECC) released the maximum mean EIRP density depending upon the frequency range as shown in Table 1.2. Apart from this, IEEE has issued Maximum Permissible Energy (MPE) levels to protect against adverse effects associated with heating the human body (Table 1.3). For human exposure to electromagnetic

Frequency of operation	Maximum EIRP density
Below 1.6 GHz	-90 dBm/MHz
1.6-3.8 GHz	-85 dBm/MHz
3.8-4.8 GHz	-70 dBm/MHz
4.8-6 GHz	-70 dBm/MHz
6 -8.5 GHz	-41.3 dBm/MHz
8.5 -10.6 GHz	-65 dBm/MHz
Above 10.6 GHz	-85 dBm/MHz

Table 1.2: Maximum EIRP density limits in Europe [5]

energy at radio frequencies from 100 KHz to 300 GHz the MPE's can be expressed in terms of local specific absorption rate (SAR).

Standard	Exposure characteristics	Frequency range	Average SAR (W/kg)	Localized SAR (W/kg) (head/trunk)
ICNIRP	Occupational	100 kHz to 100 GHz	0.4	10
	General public	100 kHz to 100 GHz	0.08	2
IEEE	Controlled	100 kHz to 6 GHz	0.4	8
	Uncontrolled	100 kHz to 100 GHz	0.08	1.6

Table 1.3: SAR Exposure Limits [6]

Definition and evaluation of SAR has been done as a part of this thesis work but for the confidentiality reasons the results are not reported. It is quite an important analysis, which explains the measure for the electromagnetic energy absorbed by biological tissue, when exposed to a radiating device. The absorption due to the microwave radiation in the UWB frequency band for low power UWB microwave cancer detection should be below IEEE exposure limit of 1.6 W/kg [6].

1.7 Organization of Thesis

→ In Chapter 2 most of the important parameters for MWI system are reported and their definitions with respect to UWB radar are presented. The concepts discussed in this chapter are not new, however by using accurate equations, link budget calculations have been performed to show how important parameters such as gain and efficiency of an antenna play a role in enhancing the dynamic range of the radar.

→ Chapter 3 is a review of existing antenna literature for medical imaging applications. Three antennas have been adapted and characterized to evaluate the compatibility with the posed requirements in chapter 2. This chapter also shows, why the parameters listed in chapter 2 are useful to evaluate and design a new antenna design aimed at imaging applications.

→ Chapter 4 presents a new novel leaky antenna structure. Extensive simulations have been performed on this antenna to verify that it fulfills the requirements imposed for this thesis application. Every parameter addressed in chapter 2 are detailedly discussed.

→ Chapter 5 presents a summary and a general assessment of the work achieved in this thesis while also discussing possible future research directions.

Requirement for UWB Radar and Link Budget Evaluation

2

2.1 Introduction

The design of a radar for detecting tumors in the human body starts by the translation of the desired performance into a set of requirements for the overall system. Such requirements are then translated into specifications for each sub system. There are several important parameters when designing an antenna which play a crucial role in the system design. We shall discuss in this chapter the important parameters needed for characterizing an UWB antenna .

2.2 Definition of Bandwidth

According to the FCC any device that exhibits a fractional bandwidth greater than 0.2 or occupies a bandwidth of 500 MHz or more of the frequency spectrum regardless of the fractional bandwidth is said to be an UWB device [19]. Bandwidth for each and every application changes in terms of determining parameters such as radiation patterns, polarization and side lobe levels. According to Balanis [20] "The bandwidth of an antenna is defined as: the range of frequencies within which the performance of the antenna, with respect to some characteristics, conforms to a specified standard". Unless specifically mentioned definition of bandwidth in this thesis is considered as S_{11} less than -10 dB.

2.3 Definition of Cross Polarization

The use of orthogonal polarizations to provide two communications channels for each frequency band has led to interest in the polarization purity of antenna patterns. There is no univocally accepted definition of cross - polarization, and in 1973 Ludwig [21] presented three different definitions that have been used either explicitly or implicitly in the literature. The IEEE standard [22] definition of cross polarization is "The polarization orthogonal to a reference polarization." For circular polarization this is adequate, but for linear or elliptical polarization the direction of the reference polarization must still be defined.

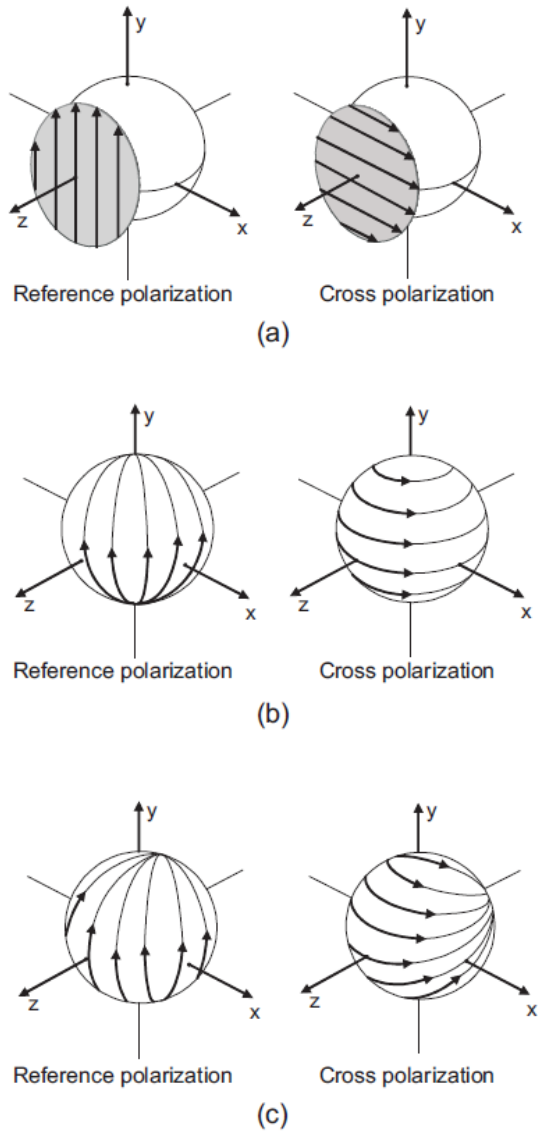

Figure 2.1: Definitions of Reference (Co) Polarization and Cross polarization for the three definitions of Ludwig. a) First definition , b) Second definition , C) Third definition.

The Ludwig third definition are generally well accepted by the antenna community and has practical significance [21]. For any linear polarized antenna (for example : short dipole) the worst case of cross polarization is observed in the diagonal planes ($\phi = 45°$ $\theta = 45°$) [23]. The most commonly used pattern measurement method is implemented by considering an antenna being placed at the origin of the system as illustrated in Fig. 2.1. Each pattern cut begins at $\theta = 0$ and the probe traversing a circle by varying θ.

This is equivalent to :

$$i_{ref}^{(3)} = \sin\phi\hat{i}_\theta + \cos\phi\hat{i}_\phi \tag{2.1}$$

$$i_{cross}^{(3)} = \cos\phi\hat{i}_\theta - \sin\phi\hat{i}_\phi \tag{2.2}$$

2.4 Definition of Antenna gain

The gain G of an antenna is the ratio of the radiation intensity U in a given direction and the radiation intensity that would be obtained, if the power fed to the antenna were radiated isotropically P_{input}.

$$G(\theta,\varphi) \quad = \quad 4\pi\frac{U(\theta,\varphi)}{P_{input}} \tag{2.3}$$

However, there are various sources for antenna system loss which contributes to the degradation of gain such as :

- ◇ Losses due to impedance mismatches.
- ◇ Losses due to the transmission line.
- ◇ Conductive and dielectric losses in the antenna.
- ◇ Losses due to polarization mismatches.

According to IEEE standards the antenna gain does not include losses due to impedance or polarization mismatches. Therefore the antenna gain only accounts for dielectric and conductive losses found in the antenna itself. However considering the definition of Balanis [20] in respective to antenna gain one can include impedance mismatch as part of the antenna gain. The antenna gain relates to the directivity (D) through a coefficient called efficiency.

$$\eta = e_p e_r e_c e_d = \eta_t \tag{2.4}$$

where

- ◇ e_p =polarization mismatches.
- ◇ e_r =reflection efficiency.
- ◇ e_c = conduction losses.
- ◇ e_d = dielectric losses.

In this thesis for the re-simulated antennas and for the newly developed antenna for the tumor detection in the human body, we considered only reflection efficiency and neglected the remaining efficiency terms. So, the gain of the antenna in this thesis is considered as :

$$G = e_r D \tag{2.5}$$

It should be observed that all quantities are angular dependent, if not otherwise said in the equation 2.5 we will consider the maximum of the parameter values within operating conditions.

2.5 Frequency Domain Analysis - Time Domain Analysis

The link between a transmitting and a receiving antenna can be characterized in terms of its complex transfer function H(f)= $\frac{U_{RX}}{U_{TX}}$ where U_{RX} and U_{TX} are the measured received and transmitted voltages (amplitudes) respectively. The dimensions of the transfer function is in meter, and they are equivalent to effective antenna heights, dependent on the frequency [24]. The coupling parameter in the frequency domain, S_{21} (ω, θ, ψ), is linked to the complex transfer function of the antennas involved in the link as :

$$S_{21}(\omega, \theta, \psi) = H_{TX}(\omega, \theta, \psi) H_{RX}(\omega, \theta, \psi) \frac{j\omega}{2\pi r c} e^{\frac{-j\omega r}{c}} \tag{2.6}$$

where

- H_{TX} and H_{RX} are the transfer functions of the transmit and receive antenna.
- r represents the distance between the two antennas.
- ω is the angular frequency.
- $j\omega$ is due to differentiation in the time domain.
- c is the speed of light in free space propagation.
- θ, ψ is the generic angular direction.

In this thesis, the impulse response of the link $S_{12}(t)$ is derived over a 7 GHz BW, from 3 to 10 GHz, by means of the IFT of the simulated $S_{12}(\omega)$ for the leaky slot antenna.

2.6 Fidelity Factor Analysis

The time domain characteristics of an antenna are quite important to study in order to analyze the pulse distortion of a signal. A parameter frequently used to quantify the pulse distortion is the Fidelity Factor (FF). FF is the maximum magnitude of the cross correlation between the normalized measured impulse response with an ideal response [25].

In equation 2.10 , $S_{12}(t)$ and $S_{\text{ref}}(t)$ corresponds to the normalized simulated impulse response and ideal reference signal.

$$FF = \max_{\tau} \frac{\int_{-\infty}^{\infty} |S_{12}(t)| \, |S_{ref}(t-\tau)| \, dt}{\sqrt{\int_{-\infty}^{\infty} |S_{12}(t)|^2 dt} \sqrt{\int_{-\infty}^{\infty} |S_{ref}(t)|^2 dt}} \tag{2.7}$$

In the equation 2.10 , the reference signal S_{ref} (t) will be a sinc associated to the mentioned 7 GHz band, which can be expressed as:

$$S_{ref}(t) = FT^{-1}\left[S_{ref}(\omega)\right] = \frac{1}{2\pi} \int_{\omega_1}^{\omega_2} e^{-j\omega t} d\omega \tag{2.8}$$

where $\omega_1 = 2\pi \times 3$GHz and $\omega_2 = 2\pi \times 10$ GHz.

FF expresses the similarity between two signals. When the two signals are exactly the same, the FF coefficient becomes unity, i.e FF = 1 . This means that 100% of the power is delivered to the receiving antenna by the transmit antenna without causing any distortion. If FF is ≤ 0.7 almost half of the power is lost during transmission process which impacts the whole radar system. In equation 2.10 the two signals have been normalized by the 2-norm in order to have unit energy and the delay τ is varied in order to find the maximum of the integral. It has to be remembered that FF characterizes only the correlation between the two signals, because of the normalization the amplitude is lost.

Since the transmission performance between two of the antennas is a critical factor in the imaging application and due to a lack of suitable reference antenna, the FF and transmission response of the antenna under test were found by simulating the transmission between two identical antennas of that type for all the simulated antennas subjected in this thesis.

2.7 Definition of Phase Center

Phase center of an antenna at a given frequency is a geometrical point in space where the radiated electromagnetic waves starts spreading spherically outward with phase being equal at any point on the sphere. Characterizing the phase center of an antenna is quite important in UWB frequency region because a change in the phase center over frequency consistently disturbs the performance of the radar and translates into processing losses.

2.8 Definition of Range Resolution

The range resolution of a radar is determined by the transmitted pulse bandwidth and is given as

$$R_X = \frac{c_0}{2 * BW} \tag{2.9}$$

where R_X is the range resolution and c_0 is the free space velocity and BW represents the effective bandwith of the transmitted signal. If the antenna operates in a dielectric medium then the range resolution becomes

$$R_X = \frac{c_0}{2 * BW * \sqrt{\epsilon_r}} \tag{2.10}$$

where ϵ_r is the dielectric constant of the medium in which the antenna is being placed. Larger bandwidth corresponds to higher resolution (smaller radar range resolution cell) , which enhances the chance of being able to detect finer targets or more details. In this thesis application , the size of the tumor of 5 mm is considered as benchmark.

2.9 Link Budget Analysis:

Resistively loaded dipoles have been used for decades to realize phase center stable broadband antennas for various applications. According to state of the art publications it is safe to assume that UWB operation of dipoles with stable phase center can be achieved with loading that

implies a maximum of 30% efficiency[26]. The reason to do link budget analysis is to have a clear understanding whether there is a real need to realize a new antenna to replace resistively loaded dipoles.

2.9.1 Elementary Efficiency Consideration

In this context elementary efficiency consideration has been performed. The effect of such low efficiency antenna is self-evident in the transmit part of the front end. The maximum power that typically can be radiated into the human body is limited to 5 mW, i.e ($\int_{BW} P_g(f)df$) [6] where P_g is the power spectral density and BW represents bandwidth. In order to transmit this power, in case of an antenna with 30% efficiency, the front end need to generate 15 mW, and 10 mW of power contribute to heating the front end only. Moreover, even the receiver part of the front end is affected by the reduced received power. In fact if we assume the fields scattered by the target produces an incoming power P_i , the receiver signal is at the most be $P_r = P_i \times 0.3$. Thus an overall power budget compensation of 10 dB higher is required by elementary efficiency considerations.

2.9.2 Signal to Noise Ratio Based System Design

To evaluate the order of magnitude of the received signal it is appropriate to quantify various terms that contribute to the received signal. The spectral power density, as a function of the frequency can be expressed as[20]

$$P_r = \frac{\eta_t D_t.\eta_r.D_r.P_g(f).\sigma.\lambda^2}{(4\pi)^3.r^4.L_{\text{propagation}}} \tag{2.11}$$

In the above equation (2.14)

- η_t, η_r stand for transmitted and received efficiency of the antenna.
- D_t and D_r represents transmitted and received directivities of the antennas respectively.
- $L_{propagation}$ is for propagation losses.
- σ stands for radar cross section [m^2]
- and r is the distance (range) between transmitted and received antennas [m].
- λ is the wavelength in free space.

We can evaluate the received power by integrating the spectral power density.

From the point of view of noise at the input of the receiver , there are various noise contributions added up for the degradation of Signal to Noise Ratio (SNR) which can be measured in terms of noise temperature and noise figure. They are the measure for the degradation of the SNR, caused by the components in the Radio Frequency (RF) signal chain, for a given bandwidth. The contribution of noise in the input of the receiver is due to number of contributions :

- ◇ The first contribution is due to the noise picked up by the antenna within its effective aperture. Eventually the noise is characterized by one parameter indicated as the antenna temperature: T_B. This parameter accounts for the radiometric power received at the antenna input due to contributions from the brightness of the entire field of view covered by the antenna.

- ◇ There is a noise contribution due to the fact that the antenna has non unitary efficiency. This contribution should be the same as that of a resistor kept at a certain physical temperature in a circuit : T_{antenna}.

- ◇ The final important noise contributor is the receiver itself. Typically the noise introduce by the receiver is characterized at the input of the receiver itself, assuming that, apart from this contribution, the receiver is noiseless. The noise of the receiver can typically be characterized by a receiver temperature: T_{receiver}.

The precise definition and possible evaluation of the antenna temperature is given in appendix A. Detailed discussion on brightness temperature and noise in the circuits is done. The noise contribution in the receiver is not discussed in this thesis.

The reason to discuss about the noise contribution in this thesis application is that, before the analysis of system noise temperature it was earlier understood that $T_{antenna}$ has a role in dimensioning the power budget of the radar.

After the detailed analysis done on the system temperature calculations which is elucidated in Appendix A, for this particular application, it was understood that the total system noise temperature $T_{system} = T_B$ i.e the noises propagated from the outside are dominated, rather than that introduced by receiver. To say briefly in mathematical terms :

$$T_B >> T_{physical}\left[1-\eta\right] + \sum_N T_{amplifier} \tag{2.12}$$

However as said earlier the overall power budget dimensioning is 10 dB higher when resistor loaded antennas (due to efficiency of the antenna) are used leading to low dynamic range radar.

Now the noise $N(f)$ in input of the receiver should be compared with signal in input of the receiver S (f). The signal in input is clearly $S(f) = P_r(f)$.

Overall the total noise in input to the receiver can be expressed as :

$$N(f) = k_B(T_{\text{B}} + T_{\text{antenna}} + T_{\text{receiver}}) \tag{2.13}$$

where k_B stands for Boltzmann constant [J/k]

Signal - to - noise ratio is defined as the power ratio between a desired signal (P_r) and the back ground noise (P_{noise}). This is equivalent to :

$$SNR = \frac{P_t.G_t.A_{\text{ant}}.\sigma.T_{int}}{(4\pi)^2.R^4.L_{\text{prop}}.L_{\text{sys}}.N_F.k_B.T_o} \tag{2.14}$$

where

$$G = \eta D_{Antenna} = \frac{4\pi A_{ant}}{\lambda^2} \tag{2.15}$$

and $\sigma = A \times\ D \times\ Refl$, Here σ is the radar cross section [m^2] of a scatterer (tumor). In equation 2.18, A_{ant} is the effective aperture of the receive antenna.

It should be observed that all quantities are angular dependent, if not otherwise said in the following Table 2.1 we will consider the maximum of the parameter values within operating conditions.

The rest of the variables in equation 2.17 is elucidated in the below Table 2.1

Variables	Representation
P_t	Transmitted power [W]
G_t	Gain of the transmitter (Single element)
A_{ant}	Effective area of the receive antenna [m^2]
A	Area of the scatterer [m^2]
D	Directivity of the scatterer [m]
Refl	Reflection coefficient of the scatterer.
T_{int}	Coherent integration time [s].
R	Distance of the scatterer [m]
L_{prop}	Propagation losses.
L_{sys}	System losses (Processing losses)
N_F	Noise figure.
k_B	Boltzmann constant [$1.38 \times\ 10^{23}$ J/K]
T_o	System (Surface) Temperature [K]
SNR	Signal to noise ratio.

Table 2.1: Parameters for SNR Calculations

For the calculations the following assumptions are made :

- ◇ Regulation : $P_t = -20$ dBW/cm^2 according to IEEE Std C95.1 , 1999 edition and -23 dBW/cm^2 according to International Commission on Non Ionizing Radiation Protection (ICNIRP) guidelines.[6]
- ◇ ICNIRP guideline used with 1cm^2 transmit antenna area.
- ◇ Only one transceiver will transmit at a time.
- ◇ Worst case : Only one receiver is switched on. Best case : 10 receivers in parallel.
- ◇ Antenna area on receive set to 1.5 cm by 3 mm.
- ◇ Area of tumor is based on width and height of 5 mm.
- ◇ Scatterer is a sphere (i.e. tumor) hence no directivity.

◇ Reflection based on difference in permittivity ϵ

$$Refl = \left[\frac{n_1 - n_2}{n_1 + n_2}\right]^2 \tag{2.16}$$

where $n_i = \sqrt{\epsilon_i}$ and ϵ_r for tumor equals to 55 for surrounding glandular tissue 50 (set to 45 for improvement calculation)

◇ Shortest integration time 0.1 seconds up to 10 seconds.

◇ Tumor in the middle of the area of interest.

◇ Propagation losses estimated by Varotto and Staderini [27] are between -40 to -60 dB (absorption and internal reflections).

◇ System losses mainly due to processing losses : approximately between 10 to 20 dB

◇ Noise factor of 5 dB (Worst case)

◇ Skin temperature is considered as 290 K

All the above assumptions lead to the following results for a tumor inside tissue with 10% difference in permittivity.

Variables	Dimensions	Worst case [dB]	Best Case [dB]
P		-23	-23
G_t		0	7
A_{ant}	$14 \times 22mm^2$	-44	-36
A	$(0.005m)^2$	-46	-46
D		0	0
Refl		-32	-32
T_{int}	0.1 seconds	-10	-10
$(4\pi)^2$		22	22
R^4	$(0.08m)^4$	-44	-44
L_{prop}		40	40
L_{sys}		20	20
N_F		5	5
k_B	$(1.38 \times 10^{23}$ J/K)	-228	-228
T_o		24	24
SNR		-14	21

Table 2.2: SNR calculated at 3GHz for tumor detection inside human body

The above calculation for SNR is valid for this thesis application alone because of propagation losses involvement and coherent integration time. This indicates that a single transmitter-receiver pair can not detect a tumour at 8 cm depth with 0.1 seconds of integration time for all frequencies in the worst case scenario. But when considering the improvements in number of receivers and integration time the SNR already improves to

35 dB at 3 GHz which is sufficient for detection. This above calculation gives preliminary information of detecting deep lying tumors near glandular tissues.

Due to confidentiality of thesis, results in respect to analysis of 3D MRI images and extraction of data from phantom repository of Wisconsin are not reported in this thesis. However, depending upon on the available literature, extracted 3D MRI's and clinical set up developed by the University of Bristol [28] it was therefore decided to match the antenna to ϵ_r =10.2 to be in competence with the state of art.

State of the Art Ultrawide - Band Antennas in Microwave Imaging

3

3.1 Introduction

Ever since engineers started using microwave based radar for medical applications, the exploration for a suitable microwave antenna has been commenced. This chapter details about antennas reported in open literature for medical imaging applications or for other imaging applications.

3.2 Antennas Used for Medical Imaging

In this chapter seven antennas used in UWB region for imaging applications are studied. Each antenna has been realized for a specific application, but by fine tuning the antenna can be matched to a medium of $\epsilon_r = 10.2$.

3.2.1 Coaxial Monopole Antenna -University of Dartmouth

The research group lead by Meaney et al [1] first introduced a coaxial monopole antenna for imaging in the frequency region of $500 - 1700$ MHz based on tomography techniques. The antennas were constructed by removing a length of the outer conductor at one end of a rigid coaxial cable. Coaxial monopole antenna is attractive for microwave breast imaging because of its size and shape which allows it to be densely packed around an imaging target. The antennas were completely immersed in the coupling medium to avoid reflections of the skin and to improve the S_{11} matching (Fig.3.1).

The matching medium liquid used in the experimental analysis was a combination of lossy glycerin and water solution.

Authors reported that due to the mismatches between the background media (coupling medium) and the human body dielectric constant, object artifacts in homogeneous phantom images appeared as false positive detections. The most recent work of this group is devoted to improve the algorithm performance to solve the problems due to the high variability of normal tissue properties, which make tumor detection more complicated than initially thought. The major problem with tomography based techniques is that it is hard to achieve high resolution of images. From here on we will consider antennas in this chapter only used in UWB radar approaches.

3.2.2 Modified Bow-tie Antenna -Delft University of Technology

The modified Bow-tie antenna was introduced for Ground Penetrating Radar (GPR) applications in the frequency region of $0.5 - 5$ GHz [29]. Compared to earlier versions of planar

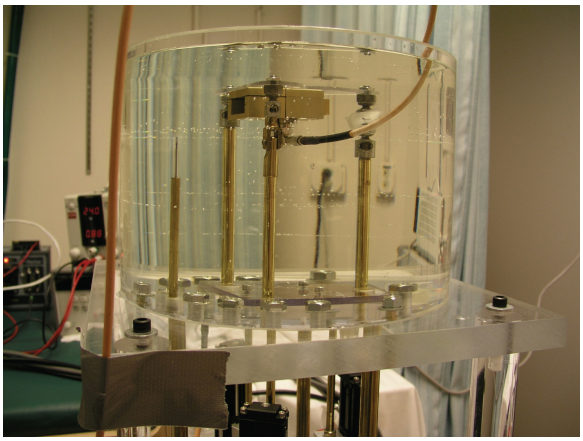

Figure 3.1: Photograph of the setup for beam pattern measurement involving a 3-point support (3PS) mechanical steering system with the aperture reference waveguide antenna positioned approximately 6 cm from the monopole transmitter[1]

resistor - loaded antennas the above mentioned antenna has improved radiation efficiency and low level of late time ringing. The antenna was realized on a FR_4 substrate to exhibit input impedance of 100 Ω in the spectrum of the exciting pulse, for matching to a 100 Ω twin semi rigid line employed as feed system (Fig.3.2). However, from the results it can be clearly seen that the input impedance was not actually matched to 100 Ω. This would have resulted high mismatch in reflection coefficient parameter in the interested frequency region [Reflection coefficient results were not mentioned in the paper]. Authors never mentioned about achieved radiation efficiency the antenna exhibited or how much % the radiation efficiency has been improved in comparison to the rest of the resistor loaded profiles. The radiation patterns in both principal planes clearly show that the antenna radiates in both the half spaces (front and back) equally leading to poor front - to - back ratio. Cross and Co - polarization levels and fidelity factor are not mentioned.

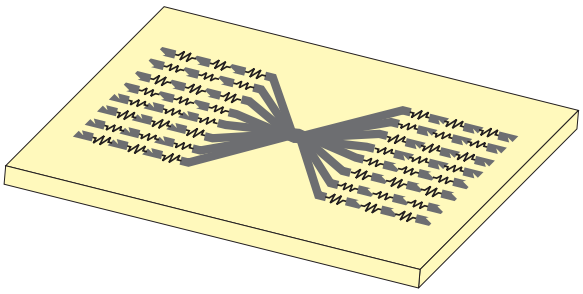

Figure 3.2: Resistor loaded antenna realized on FR_4 substrate

3.2.3 Ultra - Wideband Ridged Pyramidal Horn Antenna - University of Wisconsin

Since 1998 the group lead by Susan Hagness [30] was involved in technology development for cancer detection and in the year 2003 they introduced a novel technique based on confocal

microwave imaging for detecting tumors inside the human body. To the best of my knowledge they are the first group that proposed radar based techniques for detecting tumors based on confocal microwave imaging. The technique is based on illuminating the area of interest by arranging array of antennas either in supine or prone position over the interested region and extracting tumor response by applying time shift method. Based on the received energy from the backscattered signals an image is created as a function of location which helps to identify the tumor location.

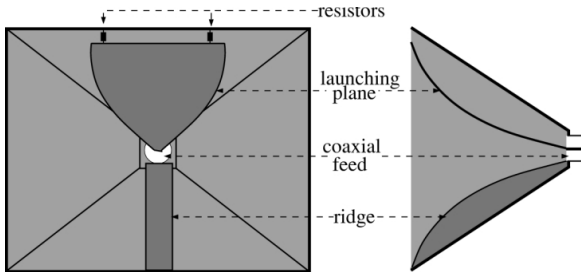

Figure 3.3: Geometry of the ridged horn antenna. (a) End view. (b) Side view.

The antenna used in the experimental analysis is a ridged pyramidal horn antenna and the frequency of operation is between $1 - 11$ GHz (Fig.3.3)[30].

3.2.3.1 Drawbacks of this Antenna

- The radiation patterns in the E plane tilts to 15° from the bore sight due to asymmetry architecture of the antenna. [30].
- Antenna efficiency is not mentioned.
- Co - polarization and Cross - polarization levels are not mentioned.

3.3 Re-simulated UWB Antennas in CST Microwave Studio

In this section three antennas mentioned in the literature for UWB applications have been re - simulated to gain physical insight in to their properties. The antennas are investigated to see whether they can be used for the medical imaging purpose and would meet the requirements set for this application as indicated in chapter 2. The antennas have been characterized in the frequency range 3.1 -10.6 GHz. The fidelity factor analysis done for the resimulated antennas in this chapter are calculated according to the equation 2.7.

3.3.1 CPW fed Circular Disc Monopole Antenna

Monopole antennas are being used since 2005 in many different forms such as elliptical [31], butterfly shaped [32] stating that they can exhibit UWB antenna characteristics. Among many existing antennas, Circular Disc Monopole antenna has been investigated in this thesis[33]. The antenna being analyzed here is printed on a FR_4 substrate ($\epsilon_r = 4.7$) with a radius r and has a thickness of 1.5 mm (Figure 3.4).

The antenna is fed by a 50 Ω microstrip feed line printed on the same side of the substrate. On the other side of the substrate, the conducting ground plane modeled with perfect electric conductor (PEC) has been printed with length L_1 covering the section of the microstrip feed line only. L and W represents the length and width of the dielectric substrate respectively and h is the distance between the feed point and ground plane.

The dimensions of this antenna are mentioned in Table 3.1

Variables	Dimensions (mm)
Length (L)	50
Width (W)	42
Radius of the circle (r)	10
Feed point distance(h)	0.3
Length of the ground plane ($L1$)	20

Table 3.1: Dimensions of CPW fed circular monopole antenna

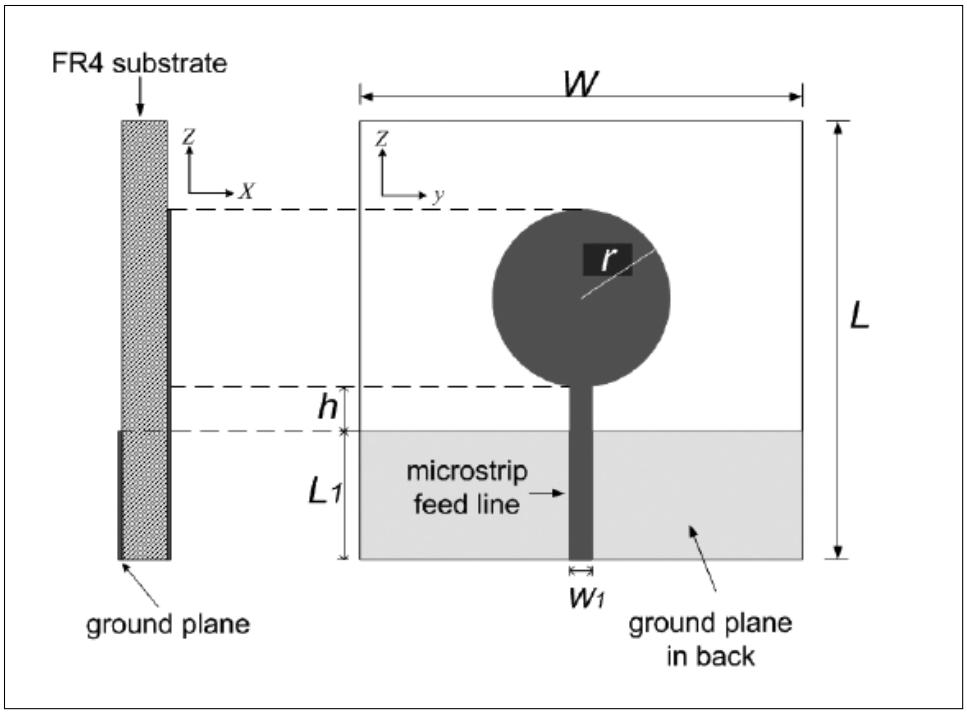

Figure 3.4: Schematic Sketch of Circular Monopole Antenna

Variations of the distance (h) resulted in different values of $S_{11} \leq -10$ dB over the frequency band. The S_{11} of this antenna for h = 0.3 mm can be observed in Fig.3.5. The important parameters in the antenna are the width of the ground plane and the dimension of the disc.

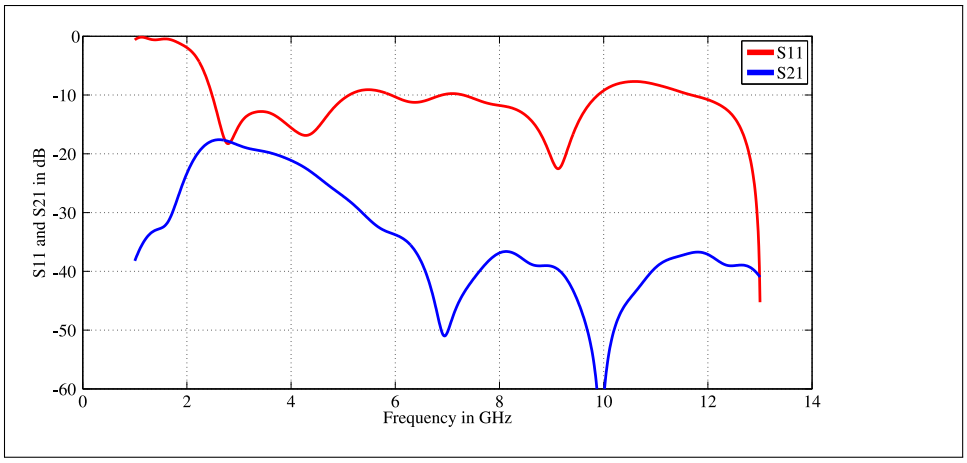

Figure 3.5: Reflection coefficient and Transmission response of Circular Monopole antenna

3.3.1.1 Cross - Polar levels at Diagonal Planes

The co and cross - polarization patterns plotted for the diagonal planes (Fig.3.6) show a null at $\theta = 0°$ and have a value of -8.2 dB for $\theta = 45°$. $(\frac{F^{45°}_{cross}}{F^{45°}_{copolar}}) = -10.174$ dB

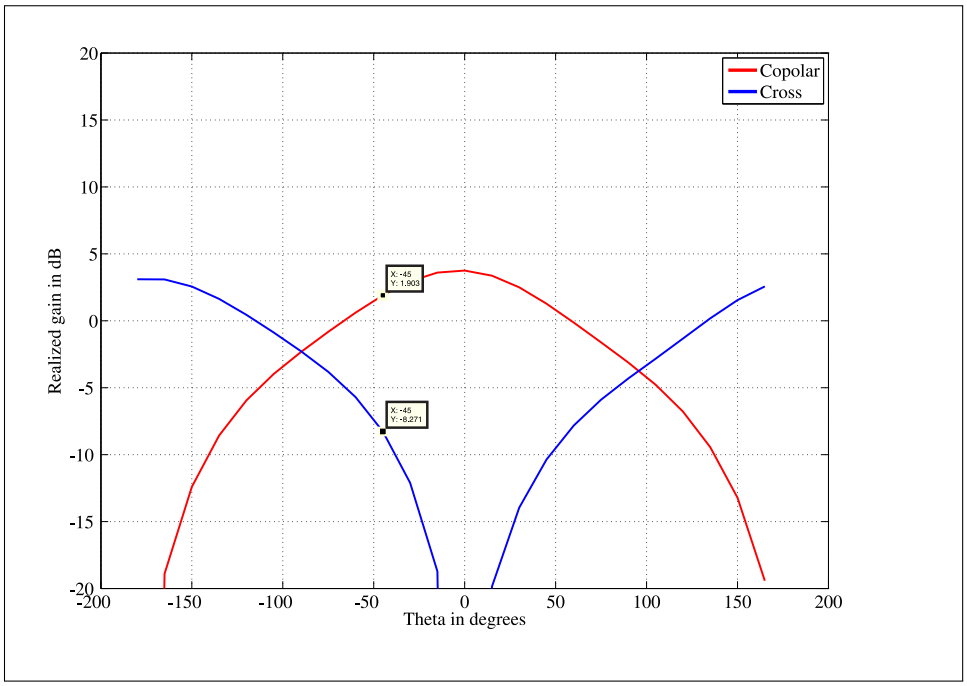

Figure 3.6: Co and Cross Polar pattern of Circular Monopole Antenna at 3 GHz

3.3.1.2 Transmission Response and Fidelity Factor Analysis

The transmission response analysis has been performed with antennas placed at 100 mm from each other in the bore sight direction. It can be observed in the Fig. 3.5 that S_{21} amplitude

in dB is not flat along the required frequency range but steadily decreases with the frequency.

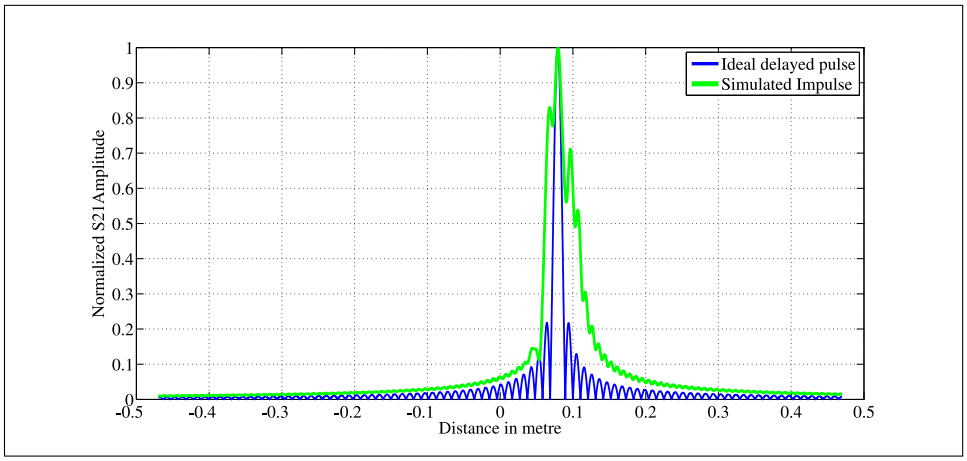

Figure 3.7: (3-10 GHz) pulse, antennas are placed at 100mm in the boresight direction, fidelity factor = 0.8

Analysis on fidelity factor has been performed (Fig.3.7) for this circular monopole antenna. The value drops to 80% in the bore sight direction indicating that almost 36% of the transmitted power is lost. Moreover, ringing is quite high and irregular shaped impulse response pattern is obtained. Except for the bandwidth matching none of the parameters recalled in chapter 2 for this particular application have been full filled.

Drawbacks of this antenna :

- High dispersiveness and low fidelity value which induces processing loss.
- Cross polarization of the antenna in diagonal planes is quite high in the higher frequency regions.

3.3.2 Integrated Blue-tooth and UWB Antenna -Polytechnic University of Catalonia, Spain

Recently, trade off studies have been conducted for incorporating UWB and blue tooth standards into single antenna geometry. In those interest lines a planar rhombic antenna geometry was introduced for UWB purpose [34]. Its simpler version has been re - simulated removing the blue tooth element from the antenna geometry (Fig. 3.8). All dimensions in Fig.3.8 are in millimetre and major geometrical details are provided in Table 3.2

Variables	Dimensions (mm)
Length (L)	42
Width (W)	48

Table 3.2: Dimensions of Modified UWB antenna

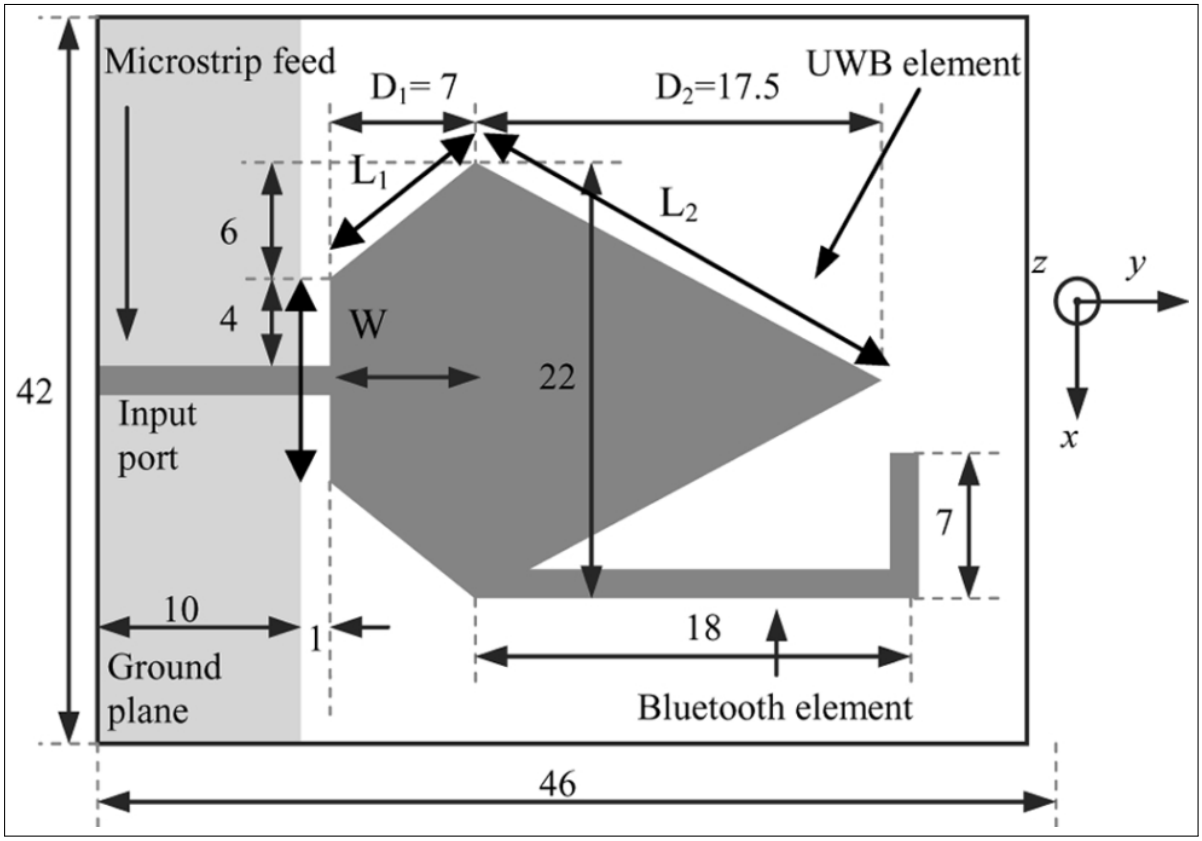

Figure 3.8: Microstrip fed rhombus shaped UWB antenna

3.3.2.1 Simulation Analysis and Matching Performance

For the simulation purpose, the antenna has been realized on a 1 mm thick FR_4 substrate with a relative permittivity of ϵ_r =4.4 and loss tangent delta of 0.02. The length and width of the substrate are given in Table 3.2 and on the other side of the substrate a 10 mm thin conducting ground plane is realized with Perfect Electric Conductor (PEC) surface in the simulations which covers the section of the microstrip line only. The feed point and ground plane are kept at a separation of 1 mm.

The matching of the antenna can be observed in the Fig.3.9. The reason for UWB performance is because of rhomboidal geometry etched on the substrate which guarantees on tapered smooth transition for the wide band response and improved matching at higher frequencies.

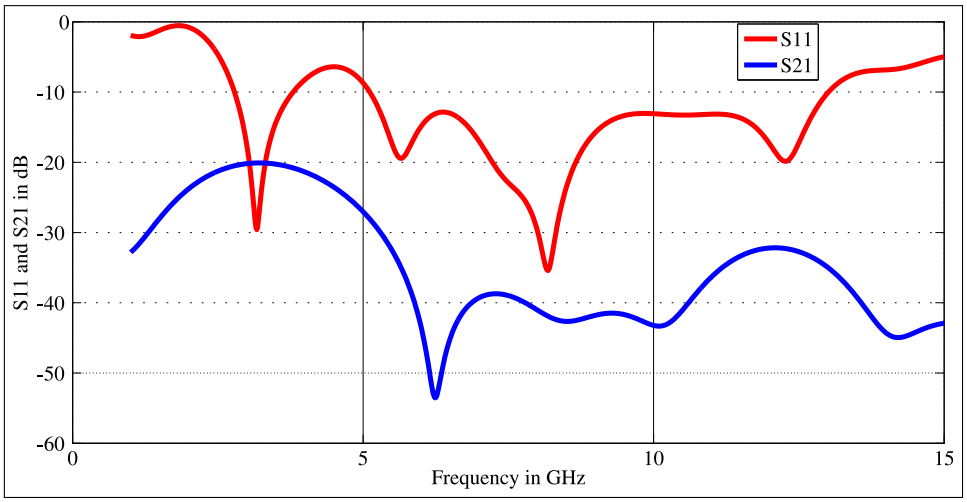

Figure 3.9: Reflection coefficient and Transmission response of Integrated UWB antenna

3.3.2.2 Radiation Patterns and Cross - polar levels

The 3D radiation patterns for this antenna (Fig.3.10) show clearly two main lobes at one of the principal plane cut (E-plane) at 7 GHz. The principal plane cuts E and H correspond to $y-z$ plane ($\phi = 90°$) and $x-z$ plane ($\phi = 0°$) planes respectively.

($\frac{F^{45°}_{cross}}{F^{45°}_{copolar}}$) observed at the diagonal plane is ≈ -11.29 dB at 3 GHz frequency, which can be seen in the Fig.3.11.

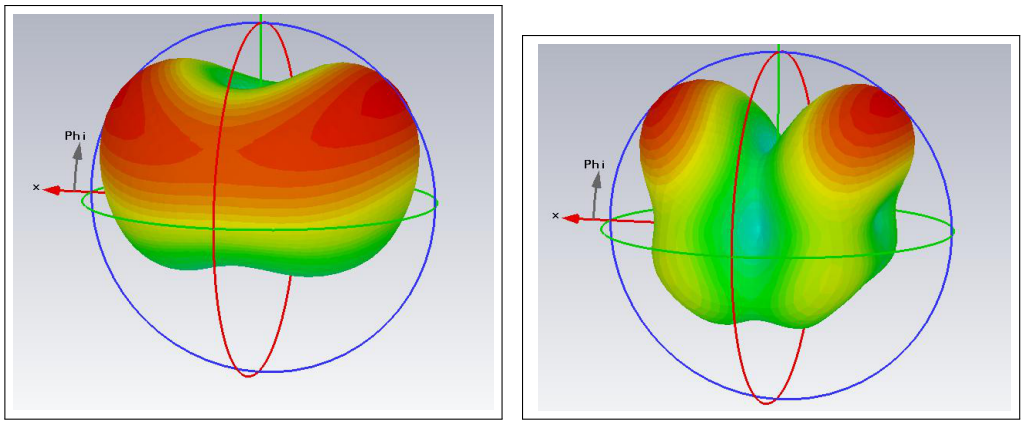

(a) 3 Dimensional Radiation Pattern at 5 GHz (b) 3 Dimensional Radiation Pattern at 7 GHz

Figure 3.10: Simulated Radiation patterns at 5 and 7 GHz for Integrated Blue-tooth and UWB Antenna

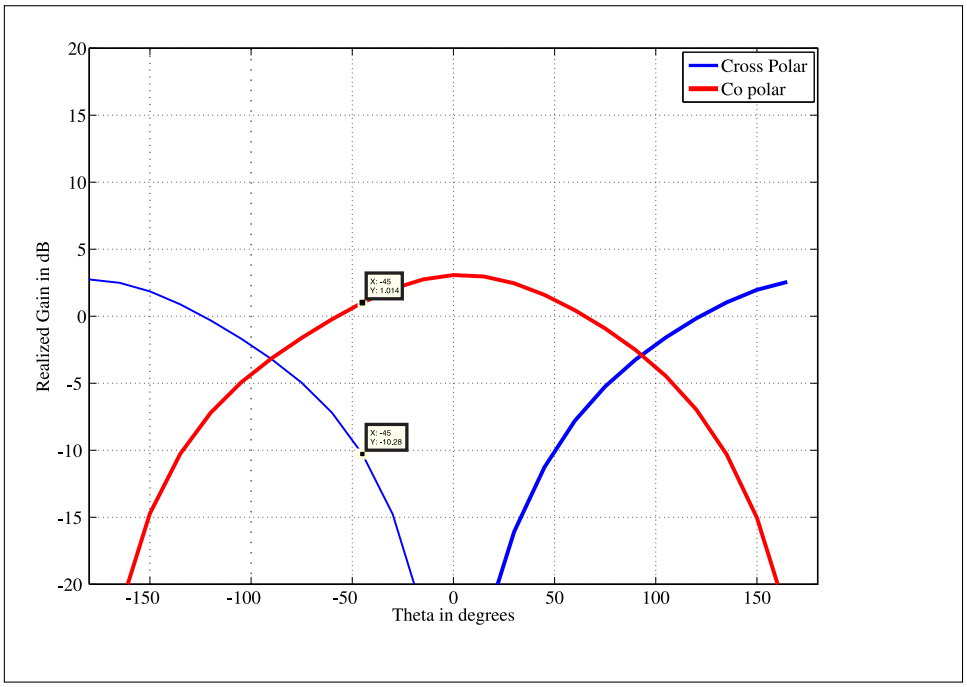

Figure 3.11: Co and Cross Polar patterns of Integrated UWB antenna at 3 GHz

3.3.2.3 Transmission response and Fidelity Factor Analysis

The transmission response analysis has been performed when antennas are placed at 100 mm apart from each other in the bore sight direction. In order to achieve minimal distortion to UWB signals transmitted into the human body, it is desirable that the magnitude of the transfer function of the antenna is flat as possible across the required frequency range. From the Fig.3.9 it is clear that the following antenna does not have such pattern but the magnitude steadily decreases with frequency (Fig.3.9). Based on this transfer function results, analysis on fidelity factor has been performed and the result can be observed in Fig.3.12.

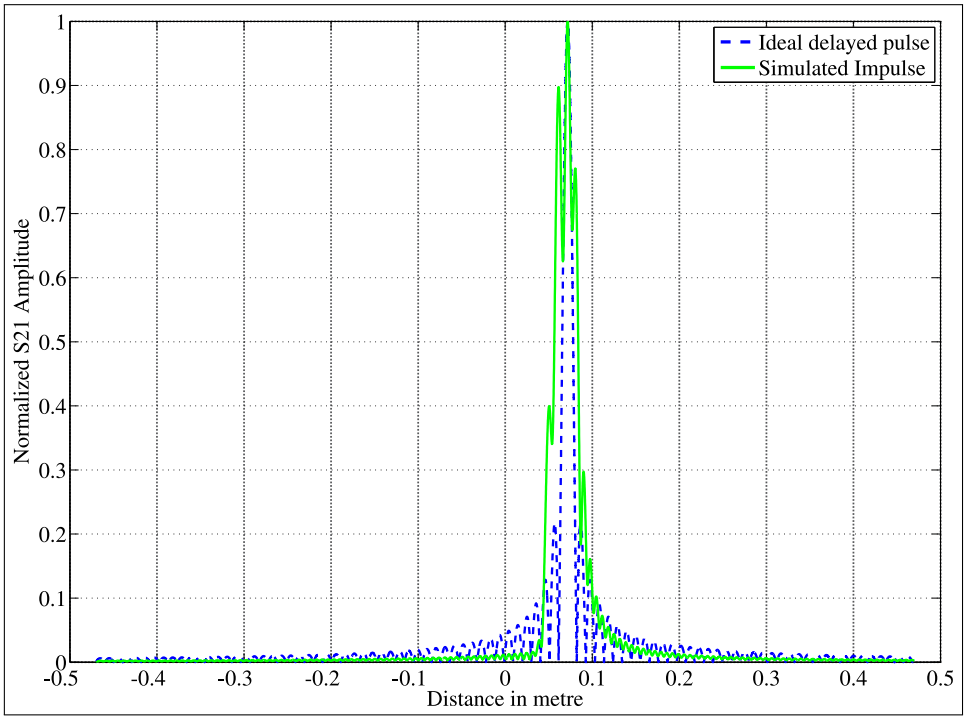

Figure 3.12: (3-10 GHz) pulse, antennas are placed at 100mm in the boresight direction, fidelity factor = 0.83

The value drops to 83% in the bore sight direction indicating that almost 28% of the transmitted power is lost. Apart from this, if we observe Fig. 3.12 ringing is quite high and irregular shaped impulse response pattern is obtained. Except for the bandwidth matching none of the parameters recalled in chapter 2 for this application have been accomplished.

Drawbacks of this Antenna are :

- ◇ Antenna radiates equally in both the planes indicating poor front to back ratio.
- ◇ Two main lobes in one of the principal planes (y-z plane) .
- ◇ Quite high dispersive antenna and low fidelity value which doesnot fit into UWB requirements list.

.

3.3.3 Wide Slot Antenna-University of Bristol

Recently, University of Bristol has been investigating the usage of microwave imaging radar in the UWB frequency region [2]. The antenna being utilized in this experiment is the fork - fed wide slot antenna. The antenna was made of dielectric substrates with a high dielectric constant ($\epsilon_r = 10.2$). Optimization was done to make antenna operate with its face immersed in a matching medium with dielectric properties similar to that of human tissue. The reason to immerse the antenna into the matching medium was to reduce the reflections between the air/skin interface. The considered matching medium has a relative permittivity varying around 9 and 10 at frequencies between 2 and 10 GHz and attenuation of 2 dB/cm at a frequency of 8 GHz [35].

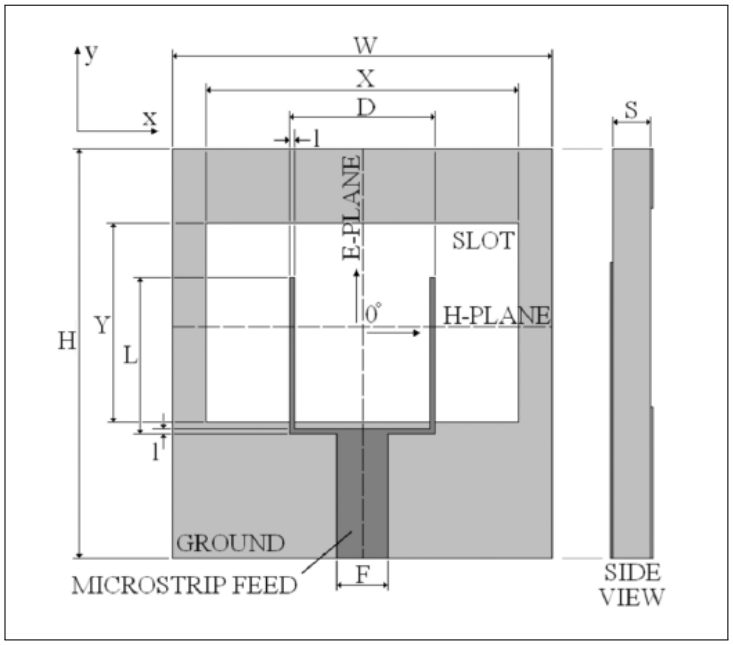

Figure 3.13: Schematic sketch of Wide slot antenna [2]

Variables	Dimensions (mm)
Length (H)	14
Width (W)	13
Height of substrate(S)	1.25
Y	7
F	1.25
l	0.2
X	10
D	4
L	6.5

Table 3.3: Dimensions of Wide slot antenna

3.3.3.1 Simulation and Matching Performance

The dimensions of this slot antenna are tabulated in Table 3.3. During simulations, the background medium ϵ_r is set to 9 and 50 mm thick block of air is attached behind the antenna to emulate true situation. The set up has been exactly considered as elucidated in [35]. The simulated S_{11} can be observed in the Fig.3.14. Considering S_{11} matching less than -10 dB the antenna can provide at maximum of 5 GHz bandwidth.

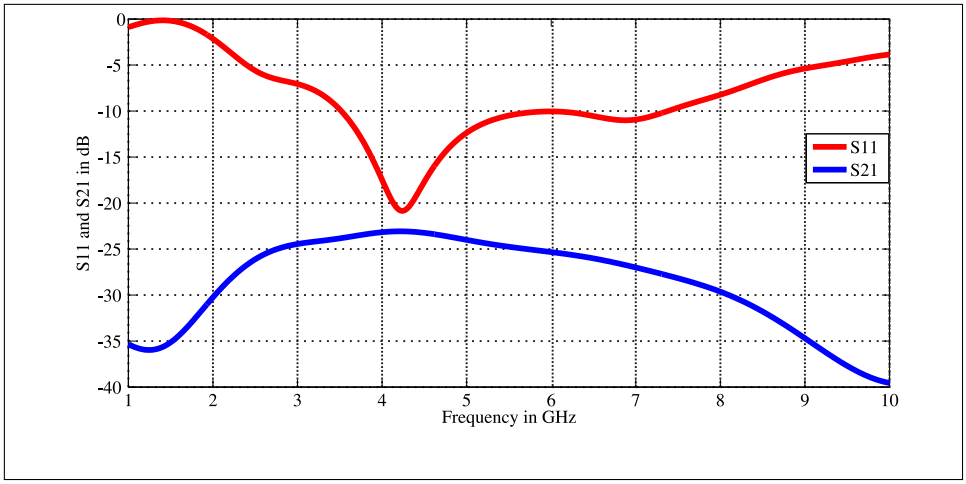

Figure 3.14: Reflection coefficient and Transmission response of Wide slot antenna

[1]

[1] *The variables in Table 3.3 are not italicized to match to the Fig.3.13.

3.3.3.2 Radiation Patterns of Wide slot antenna

The radiation patterns of the wide slot antenna are quite wide in H plane (Fig.3.15) and the patterns in the E plane tilt to 15° from the main lobe (Fig.3.16). The reason for the tilt in the E-plane main beam could be due to the asymmetric feeding of the microstrip line. −3 dB beamwidth for the wide slot antenna in both the principal planes are tabulated in Table 3.4.

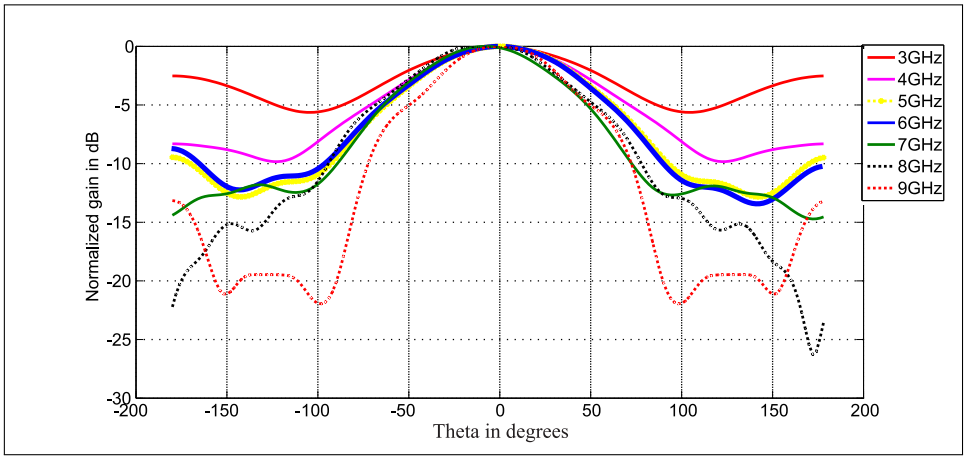

Figure 3.15: Radiation patterns of Wide slot antenna in H plane $\phi = 0°$

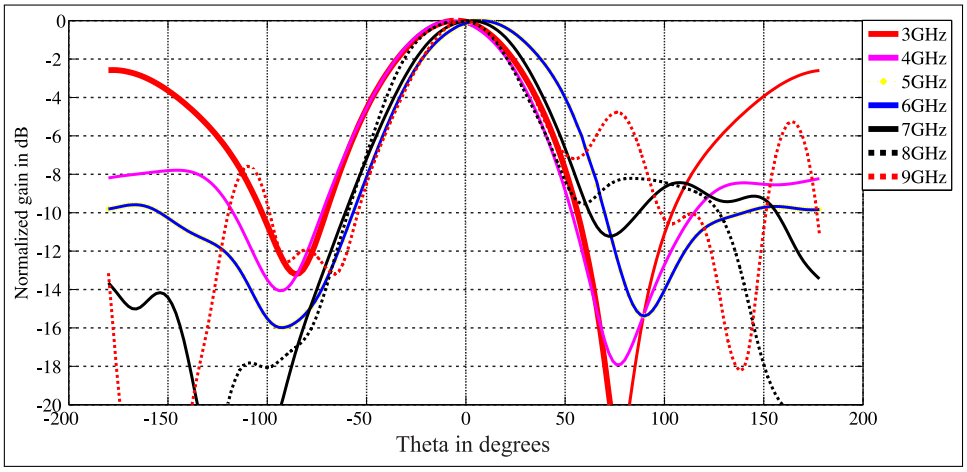

Figure 3.16: Radiation patterns of Wide slot antenna in E plane $\phi = 90°$

3.3.3.3 Cross - Polar levels at Diagonal planes $\phi = 45°$, $\theta = 45°$

The cross - polar levels for the wide slot antenna has been calculated based on the Ludwig 3 definition [21] at $\phi = 45°$, $\theta = 45°$ for all frequencies i.e 3-9 GHz reported in Table 3.5. Wide slot displays a very low cross- polar levels at lower frequencies, whereas cross- polar levels are quite high at higher frequencies.

Frequency in GHz	-3dB Beamwidth (H-plane) deg	-3dB Beamwidth (E-plane) deg	Comments
3	174.4	73.2	No beam squint.
4	114.1	72.6	Beam squints to 8° from main lobe in E-plane
5	90.3	70.8	Beam squints to 7° from main lobe in E-plane
6	84.8	66.9	–
7	88.9	59.7	Beam squints to 9.0° from main lobe in E-plane
8	74.7	57.7	Beam squints to 12.0° from main lobe in E-plane
9	69.1	54.7	Beam squints to 17° from main lobe in E-plane

Table 3.4: Beam width of Wide slot antenna

Frequency in GHz	Realized gain (1 - S_{11}^2 dB	$(\frac{F_{cross}^{45^\circ}}{F_{copolar}^{45^\circ}})$ dB
3	3.656	-17
4	6.103	-17.2
5	7.082	-13.7
6	7.422	-7.4
7	8.087	-2.5
8	8.527	-2.5
9	8.448	-4.256

Table 3.5: Gain and cross polar level of Wide slot antenna at different frequencies

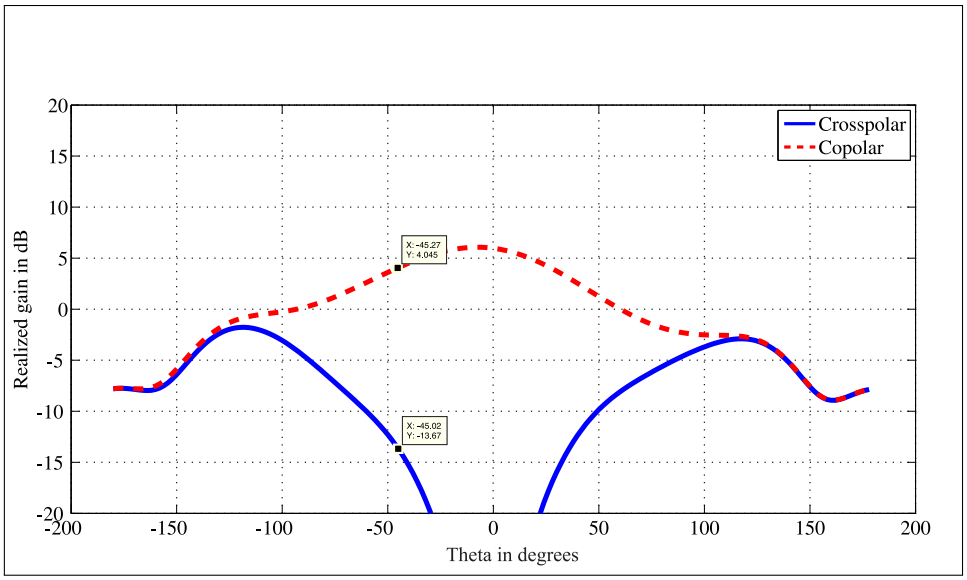

Figure 3.17: Cross polar levels at diagonal planes $\phi = 45°$, $\theta = 45°$ at 4 GHz

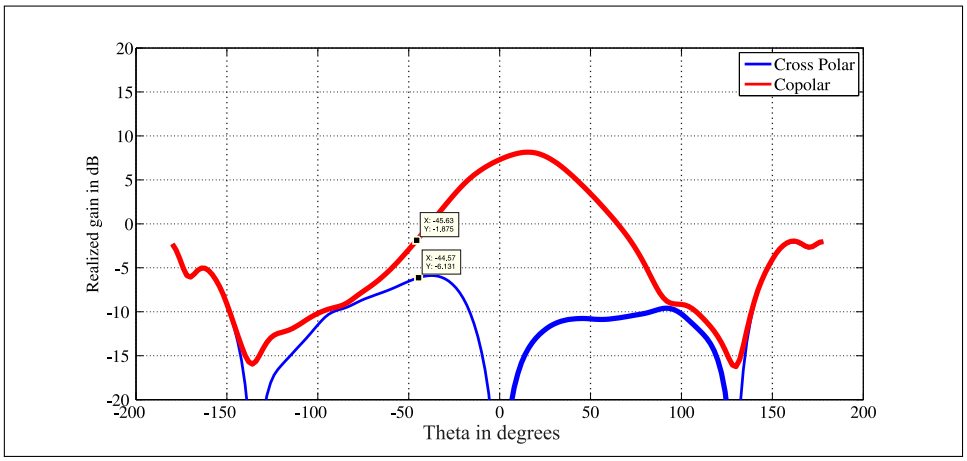

Figure 3.18: Cross polar levels at diagonal planes $\phi = 45°$, $\theta = 45°$ at 9 GHz

3.3.3.4 Transmission Response in Lossy Environment

The transfer function of the system which includes the two antennas and the channel in between has been computed when they are kept at 100 mm apart in bore sight direction for both lossless (Fig.3.14) and in lossy medium (Fig. 3.19). Because of the attenuation in the matching medium, there is a heavy drop in the signal gain (i.e S_{21} in dB) in the frequency region $3 - 10$ GHz. The dielectric properties of the medium used for evaluating the antenna performance are shown in Fig.3.20.

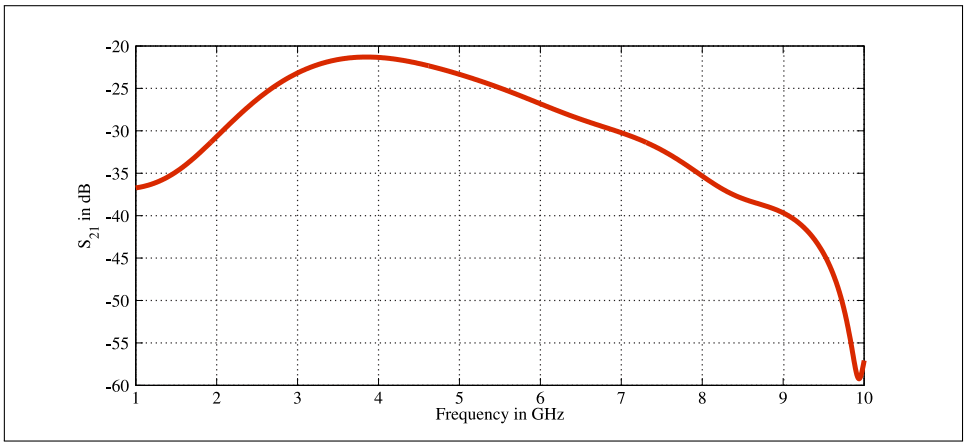

Figure 3.19: Performance of Wide slot antenna in lossy medium

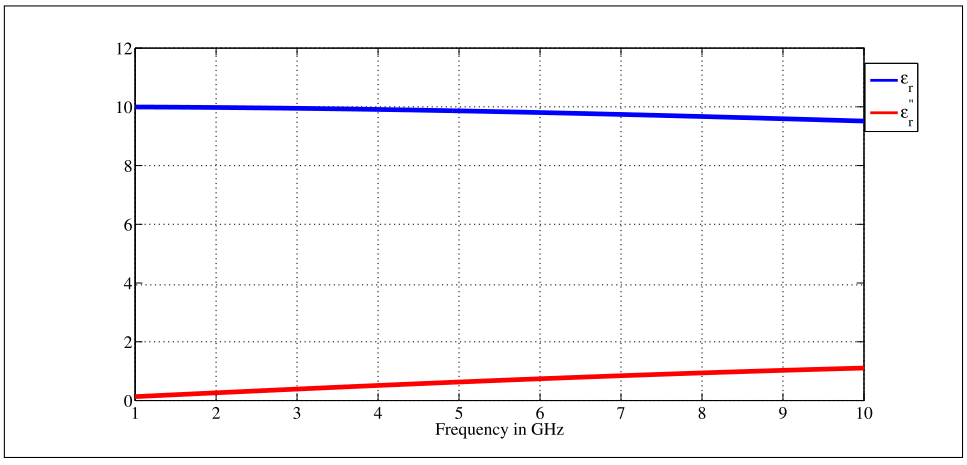

Figure 3.20: Liquid phantom medium used for microwave imaging.

3.3.3.5 Fidelity Factor analysis and Performance of Wide Slot antenna at bore - sight direction

Although the efficiency of the antenna is quite low, in order to fulfill the complete analysis of the antenna, fidelity factor analysis has been performed in the bore sight direction when the antennas are placed at 100 mm. In the bore sight direction, the value drops to 89% indicating almost 20% of the transmitted power is lost (Fig. 3.21). Moreover ringing can be observed in the simulated impulse response.

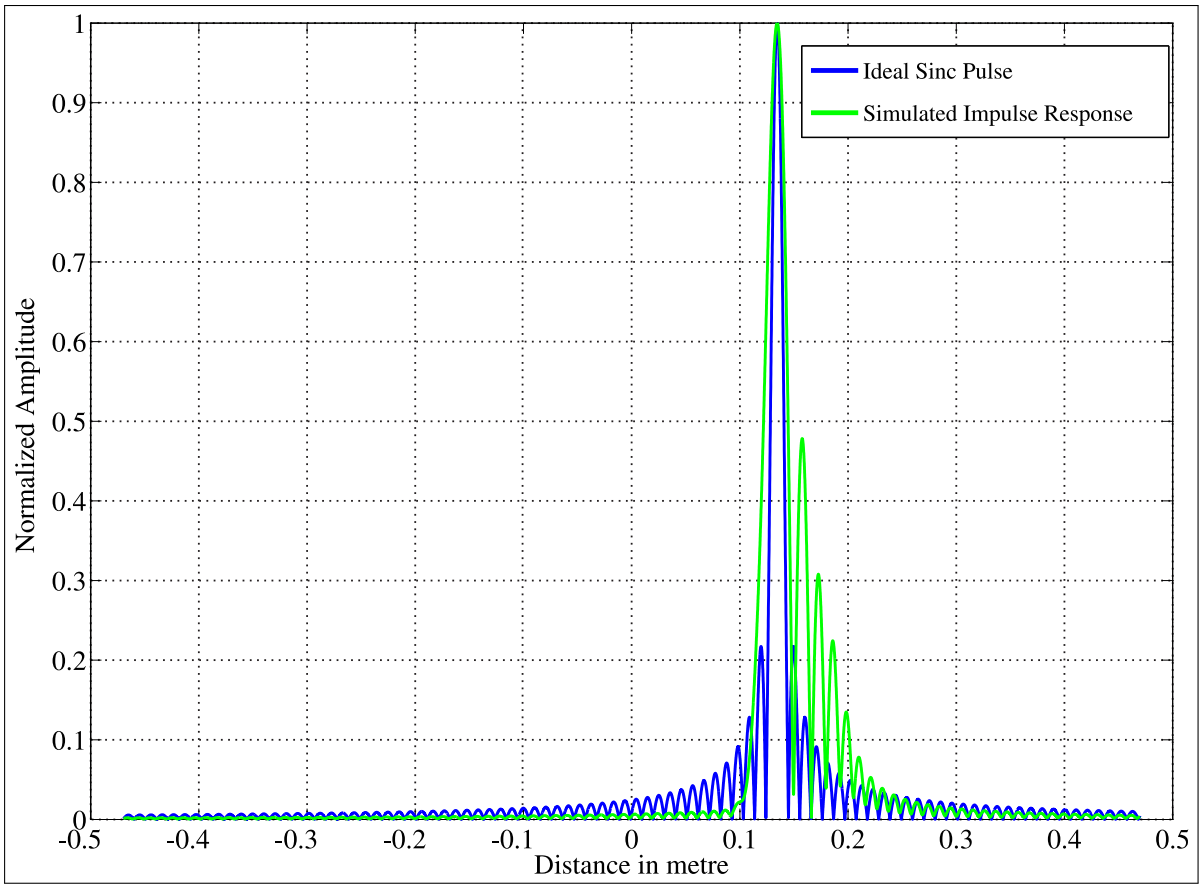

Figure 3.21: Fidelity analysis for the Wide slot antenna in the boresight direction.

Drawbacks of this Antenna :

- ◇ Efficiency of the antenna is $70 - 80\%$ approximately in the UWB frequency region.
- ◇ The main beam in E plane tilts to $15°$ from the bore sight direction.
- ◇ The bandwidth is quite low to obtain fine resolution of images.

However, this is the radiating element currently included in the system under test at Bristol Clinical Centre for detection of tumors inside the human body. Even if the antenna performance is not completely in line with parameter values listed in chapter 2, by means of extensive signal processing techniques and incorporating high number of antenna elements in the array configuration detection of tumors was demonstrated.

In view of this, development of a novel antenna which could surpass these difficulties and perform better than existing antennas appears to be necessary. In the next chapter a detailed discussion about the novel antenna developed in a cooperation between TU Delft and TNO will be elucidated.

Novel Ultra-Wideband Leaky Slot Antenna

4

4.1 Introduction to Leaky-Wave Propagation

The Green's function for an infinite slot etched between two different semi - infinite homogeneous dielectrics and fed by a short dielectric dipole has been investigated in [36] and [37]. For this structure, closed form expression for the magnetic currents has been derived together with the input impedance. The derivation for the closed form expression for the magnetic currents in [36] and [37] is summarized in the following text :

A slot of width w_s is etched along the x axis in a perfect electric, infinitely thin ground plane located on the $x-y$ plane separating two different semi infinite homogeneous dielectric half spaces (Fig. 4.1). The relative permittivities of the media occupying the region z <0 and z >0 are represented as ϵ_{r1} and ϵ_{r2} respectively. The slot is fed by a y directed impressed current (Impressed currents are analogous to ideal current generators which are normally not affected by the magnetic fields that are propagating along the slot).

Separability between the transverse and longitudinal space functional dependence is assumed for the magnetic currents $m(x,y) = v(x)\ .\ m_t(y)$. The transversal functional dependence is taken as respecting quasi-static edge singularities.

$$m_t = \frac{-2}{w_s \pi} \frac{1}{\sqrt{\left(1 - \frac{2y}{w_s}\right)^2}} \tag{4.1}$$

On the basis of this assumption a detailed procedure to find the space domain magnetic current for the leaky slot has been outlined in [36]. For a δ gap feed, the expression of the longitudinal voltage across the slot (i.e the voltage along the length of the slot) is given in analytical form as :

$$v(x,t) = \frac{1}{2\pi} \int_{-\infty}^{\infty} \frac{\mathrm{sinc}\frac{(k_x t)}{2} e^{-jk_x x}}{D(k_x)} dk_x \tag{4.2}$$

where

$$D\left(k_x\right) = \frac{1}{2\varsigma_0 k_0} \sum_{i=1}^{2} (k_i^2 - k_x^2) J_0\left(\frac{w_S}{4}\sqrt{(k_i^2 - k_x^2)}\right) H_0^2\left(\frac{w_S}{4}\sqrt{(k_i^2 - k_x^2)}\right) \tag{4.3}$$

where ς_0 and k_0 are the characteristic impedance of the free space and free space propagation constant respectively , k_i represents the intrinsic wave numbers in the two media of dielectric constant of ϵ_{r1} and ϵ_{r2}. J_0 and H_0^2 are the zero-th order Bessel and second kind Hankel function respectively.

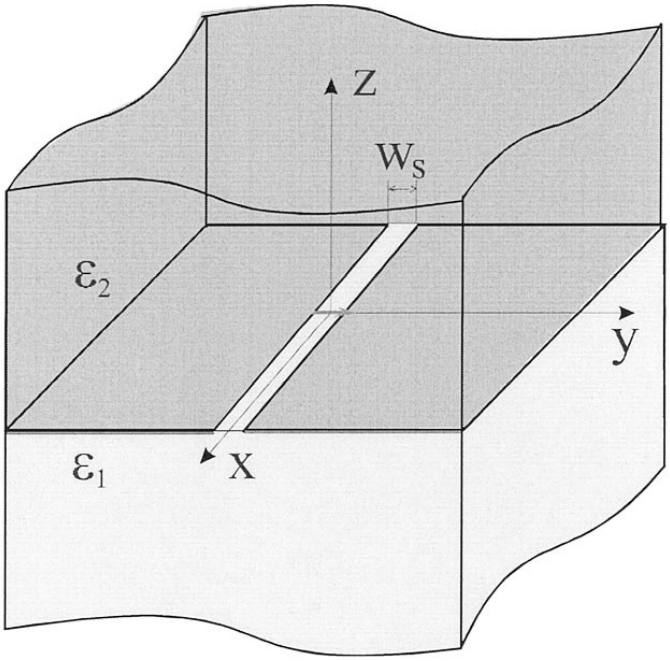

Figure 4.1: Geometry of infinite extended slot etched between two semi infinite dielectrics.

From the asymptotic expressions realized for the spectral representation of radiated fields it can be observed that at certain distance x from the source the leaky wave contribution only dominates the total field. The predominance of the leaky wave contribution is more pronounced for small slot width and for high dielectric contrasts, since it implies a weaker attenuation of the leaky wave. The leaky wave propagates along x with phase constant β=Re(k_x^{LW}) and attenuation constant δ_{LW}=Im(k_x^{LW}).

It has been outlined in [3] that leaky wave radiation is much larger phenomenon than space wave radiation when the slot is narrow in terms of wave length. "The leaky wave mode is associated to distributed radiation which occurs ONLY in the dense medium, whatever is the dielectric constant provided there is one"[3].

4.1.1 Enhanced Ultra-Wideband Leaky Lens Antenna

In [3] an enhanced UWB leaky lens antenna has been realized which had impedance matching over a decade bandwidth, stable phase center, high efficiency, uniform radiation patterns and high fidelity factor. Before we discuss about enhanced leaky lens, a further explanation to Fig.4.1 can be done based on a simplified ray picture of the near field radiated by a standard leaky slot printed at the interface between air and a dense dielectric, is shown in Fig. 4.2.

The region of co-existence of the leaky wave and the space wave, as well as the region where only space waves exist is shown in the Fig. 4.2. The Fig.4.2 also shows the leaky wave angle, γ_{LW} [3]. When the Green's function is evaluated asymptotically, it leads to different wave contributions namely space wave, a surface wave and leaky wave.

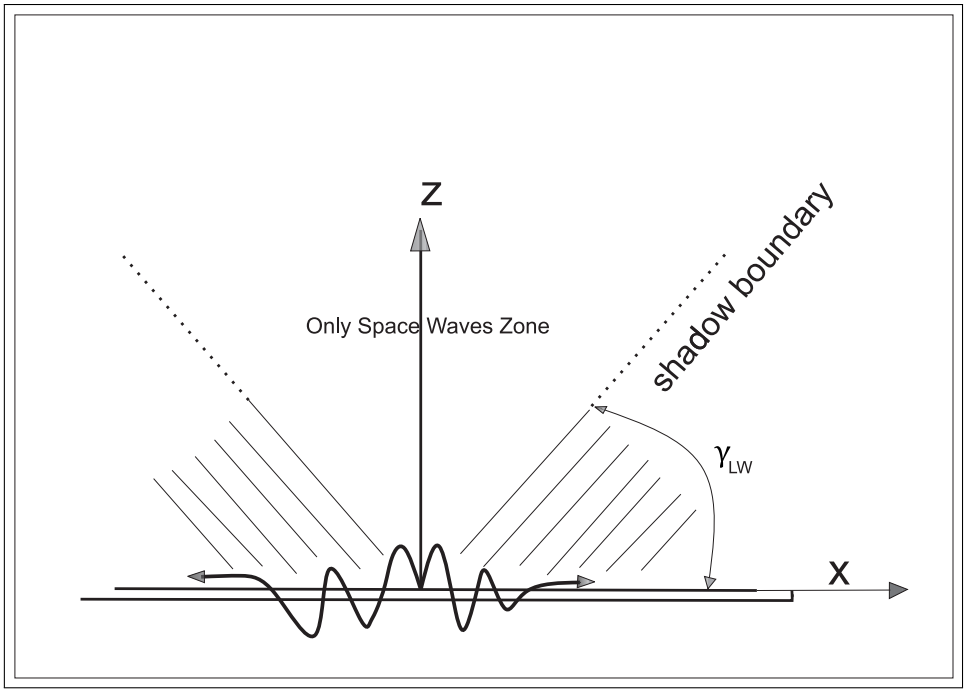

Figure 4.2: Side view of the near field ray picture showing leaky waves existence zones, and the leaky wave angle, γ_{LW} for a leaky slot antenna.

→ Surface Wave : It is the wave that propagates at the interface between two media and it decreases along z as $\frac{1}{\rho}$ where $\rho = \sqrt{x^2 + y^2}$ in the upper half space until the shadow boundary. Therefore, it does not radiate. This solution exists when the incidence angle inside the dielectric slab is larger than critical angle or when the phase velocity is smaller than the speed of the light. Hence it is called as slow wave.

→ Leaky Wave : When the incidence angle is smaller than critical angle leaky wave solution exists. This wave shows an amplification in z but only till shadow boundary. This solution can also be characterized by phase velocity inside the slab larger than the speed of light. Hence it is a fast wave.

The angle γ_{LW} of radiation of each leaky wave is associated to the real part of the propagation constant of the leaky wave propagating along the slot. In the previous developed UWB leaky lens [38] it was assumed that the propagation constant associated to this type of radiation is mainly the average of the propagation constant in the two dielectric media, i.e $\beta = \sqrt{\frac{k_1^2+k_2^2}{2}}$, where k_i (for i=1,2) is the propagation constant in the medium with dielectric constant (ϵ_{ri}) where ϵ_{r1} is characterizing the less dense medium.

Increasing the dielectric constant would always lead to an upper boundary of 45° for the leaky wave angle $\gamma_{LW} = cos^{-1}\left(\frac{\beta}{k_2}\right)$. This leads to a separation of the two beams of at least 90° when slot is fed at the central point (Fig.4.5). Although the radiation patterns obtained through this formulation yield frequency independent main beam, it also yielded higher side lobe levels with difficulty to realize in printed board circuit technology.

In [3] it was understood that if $\beta \approx k_1$ then the angle between the two beams in the denser dielectric is much smaller in comparison to [38] leading to have an unique secondary main beam with low side lobe levels. In the sense $\beta \approx k_1$ implies that waves are propagating in the dielectric with enhanced leaky wave angle. To achieve this condition it is sufficient to introduce a small air gap separation h between the slot and the dense dielectric as shown in Figure 4.3.

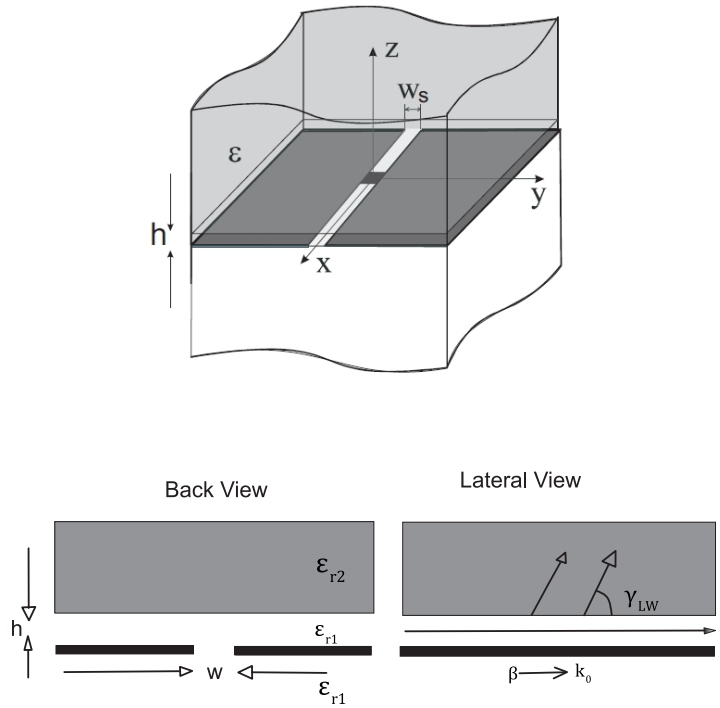

Figure 4.3: Infinite leaky slot etched between two semi infinite dielectrics with separation layer h

In order to achieve some directivity, the leaky slot antenna was used as a feed to excite a circular symmetrical elliptical lens as depicted in Figure.4.4. The performance achievable with this leaky lens antenna are promising with respect to the medical imaging application parameters listed in chapter 2 such as stable phase center, high fidelity (pulse preservation properties) , high efficiency, uniform radiation patterns, wide impedance matching. Circular symmetry of the lens lead to reasonably symmetrical patterns as demonstrated in [39] .

In this thesis application the antenna should be used in close proximity of the human body and should ensure as wide as possible main beams to uniformly illuminate the area of interest. To achieve this lens has to be removed from the antenna to avoid directivity radiation beams. If additional measures are not taken the canonical problem of this leaky slot alone without lens is that, when the slot is fed at the central point it splits the radiated power into two conical beams forming an angle γ_{LW} with the slot as depicted in the inset view of Figure 4.5.

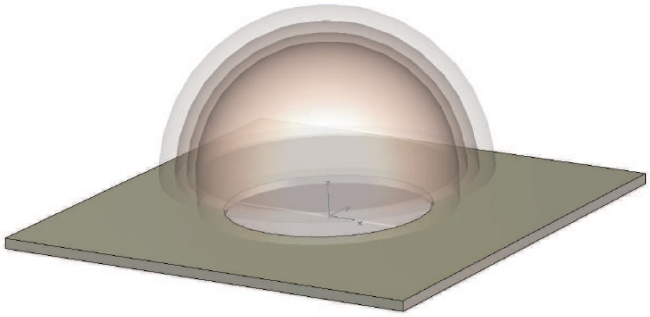

Figure 4.4: CAD drawing of the enhanced UWB Leaky Lens design [3]

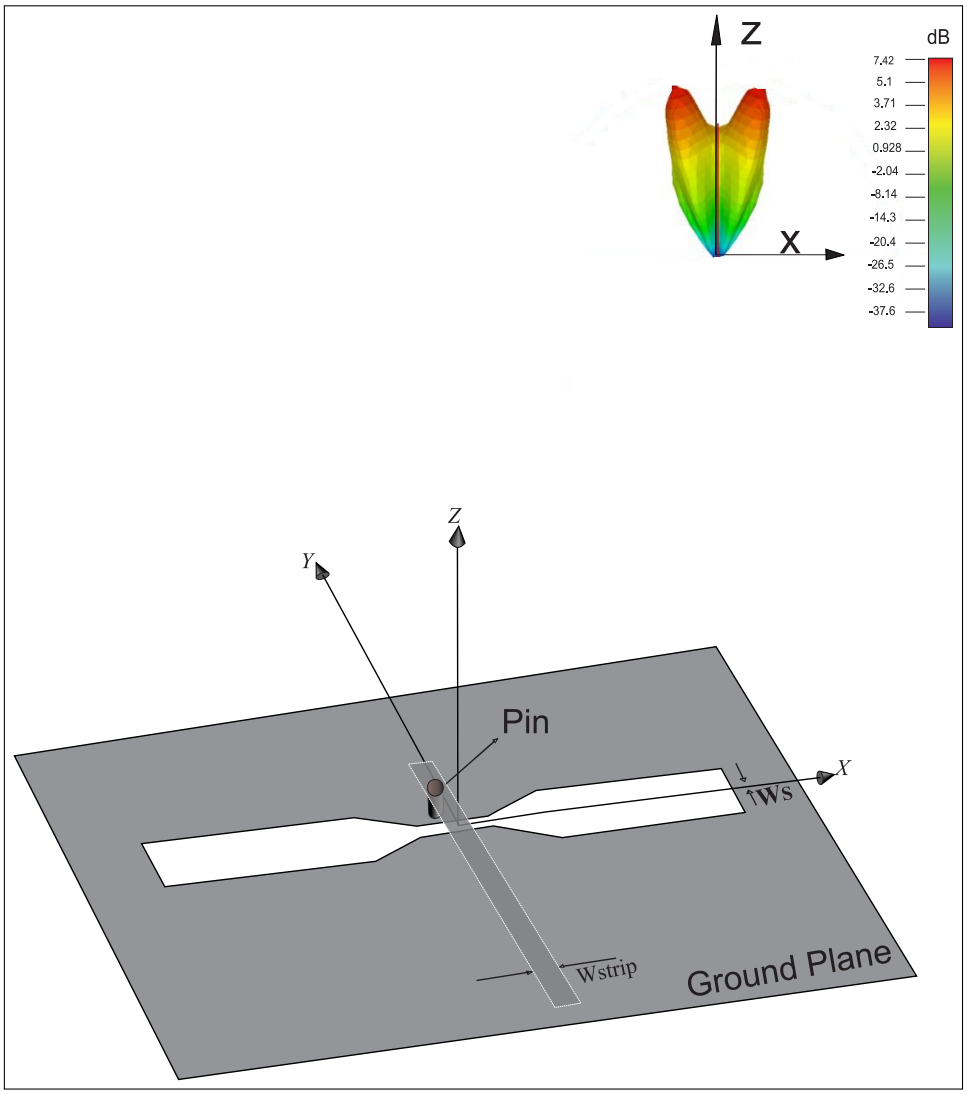

Figure 4.5: Leaky slot used for exciting circular symmetrical lens [3] and in inset view the obtained radiation pattern without lens.

4.2 Design Procedure for Novel Leaky Slot Antenna

The leaky lens antenna in [3] was designed to operate in the frequency range 20 - 60 GHz. In order to make use of leaky slot properties for our application the slot has to be scaled of a factor 6 leading to a larger structure making it not suitable directly for a system in particular when used as a element of a complete array. So to make it suitable for this application two main steps were involved in designing the novel antenna:

→ Flaring.

→ Resizing the antenna.

4.2.1 Principal Mechanism : Flaring the antenna

In order to achieve a single uniform beam in the broad side direction in absence of the lens, flaring has been applied at the both ends of the antenna in both sides along x axis.

In Fig.4.6 for different flaring configurations of the slot, corresponding radiation beams can be observed. When the slot widens up its opening angle along x axis, the two conical directive beams become broaden along z axis and over - lap with each other resulting in single main radiation beam. Based on this observation, extensive optimization has been done in CST microwave studio [40]to achieve this mechanism.

4.2.2 Slot Dimensioning

When resizing the antenna for our application additional care has been taken in optimizing the width of the slot and the air gap between the slot and the denser dielectric. It has been shown in [3] that when the values of $w_s = h$ become larger in terms of wave length the leaky beams are more directive and pointing more towards the critical angle. So, the values of w_s and h are maintained smaller in terms of wave length in order to have broad beams rather than directive beams.

When the length of the slot is quite small, the leaky wave attenuates rapidly and the whole amplification of power is done along z axis. As there was no stringent requirement on the antenna directivity , a short leaky slot was designed and realized in the operating frequency of 3 to 10 GHz .

The slot length has been fixed at 20 mm, as a compromise between performances and the size of the phantom. Indeed even if the power at the edges of the slot is still significant, the reflected power can be considered entirely radiated before it reaches the feed point again. In this way extensive optimization has been done on slot dimensioning to meet the performance requirements (Fig.4.7).

In earlier design for the leaky lens antenna a small air gap separation h between the slot and the dense dielectric was introduced to achieve unique secondary main beams with low side lobe levels. However in this application we replaced the air layer with poly tetra fluoro ethylene (PTFE) which has ϵ_r =1.96 and $\tan_\delta$ =0.0019. From here on slot with PTFE dielectric as the separation gap h between the slot and the denser dielectric would be called as LSPTFE.

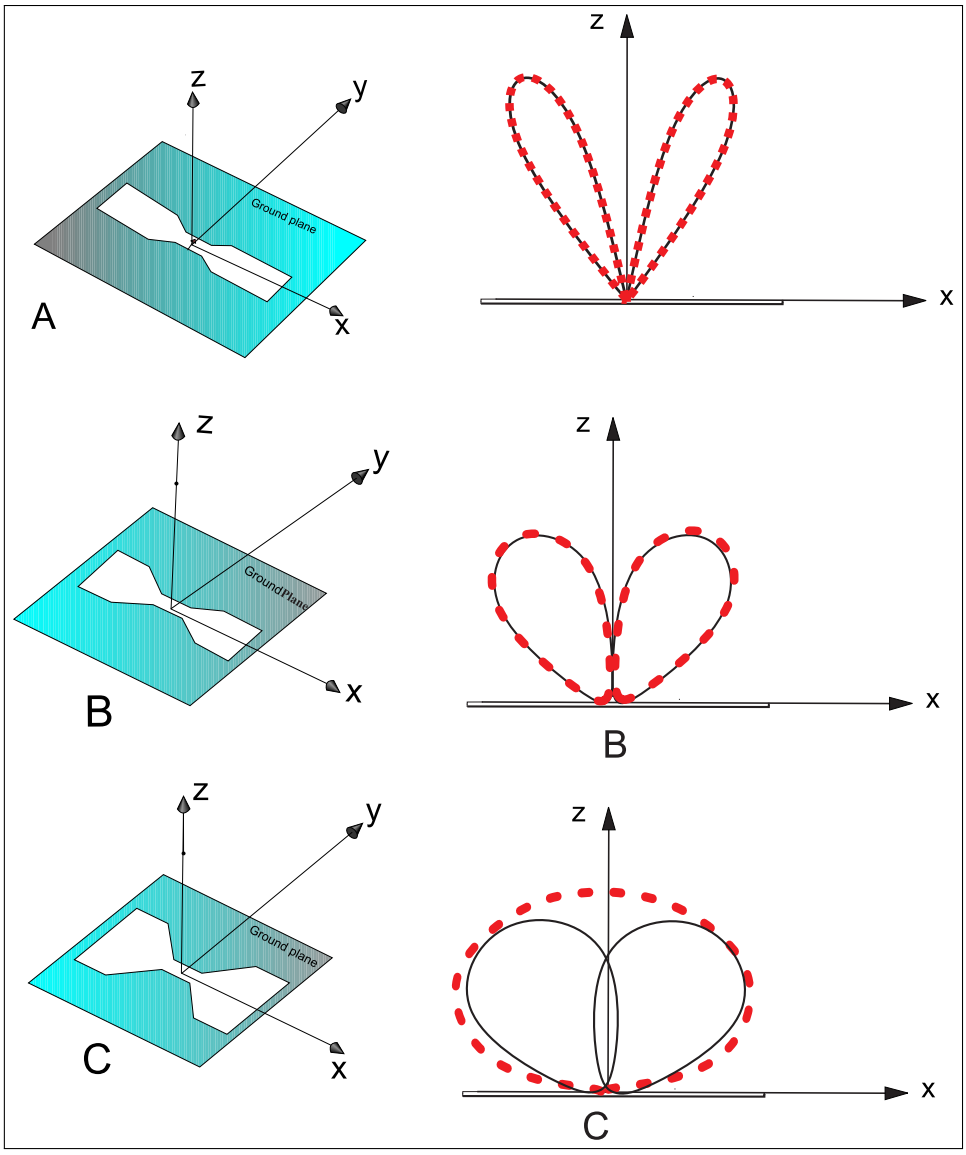

Figure 4.6: Different configurations of leaky slot antenna in terms of flaring and its corresponding conical beam radiations. [A] 1x Flaring , [B] 2x Flaring , [C] 3x Flaring, where x corresponds to the variation in the opening angle of the slot.

4.2.3 Details of the Feed

The length and width of the ground plane are denoted as L_{ground} and W_{ground} respectively. The slot length and width are denoted as $L_1 + L_{trans} + L_2$ and W_{slot}. The slot is directed along the x axis, etched in a perfect electric ground plane located on the x-y-z plane (Fig. 4.7). The microstrip feeding line is shorted to the slot's plane via a metallic pin for feeding the slot. The width of the microstrip is chosen to match the characteristic impedance of 50 Ω. The dielectric block on the top of the slot (h) (Fig.4.9) plays an important role in obtaining good impedance matching. Also, the separation gap (h) plays an important role in obtaining very good cross - polarization levels in diagonal planes.

Parameter	Value
W_{slot}	9.6 mm
$L1 + L_{trans} + L2$	11.343 +1+11.343 mm
W_{ground}	14 mm
L_{ground}	22 mm
pin	0.127 mm in diameter
$\epsilon_{\mu strip}$	3
h	0.8 mm
h_{thick}	30 μm
h_{strip}	127 μm
W_{strip}	0.32 mm
H_{Back}	50 mm

Table 4.1: Geometrical details of leaky slot antenna

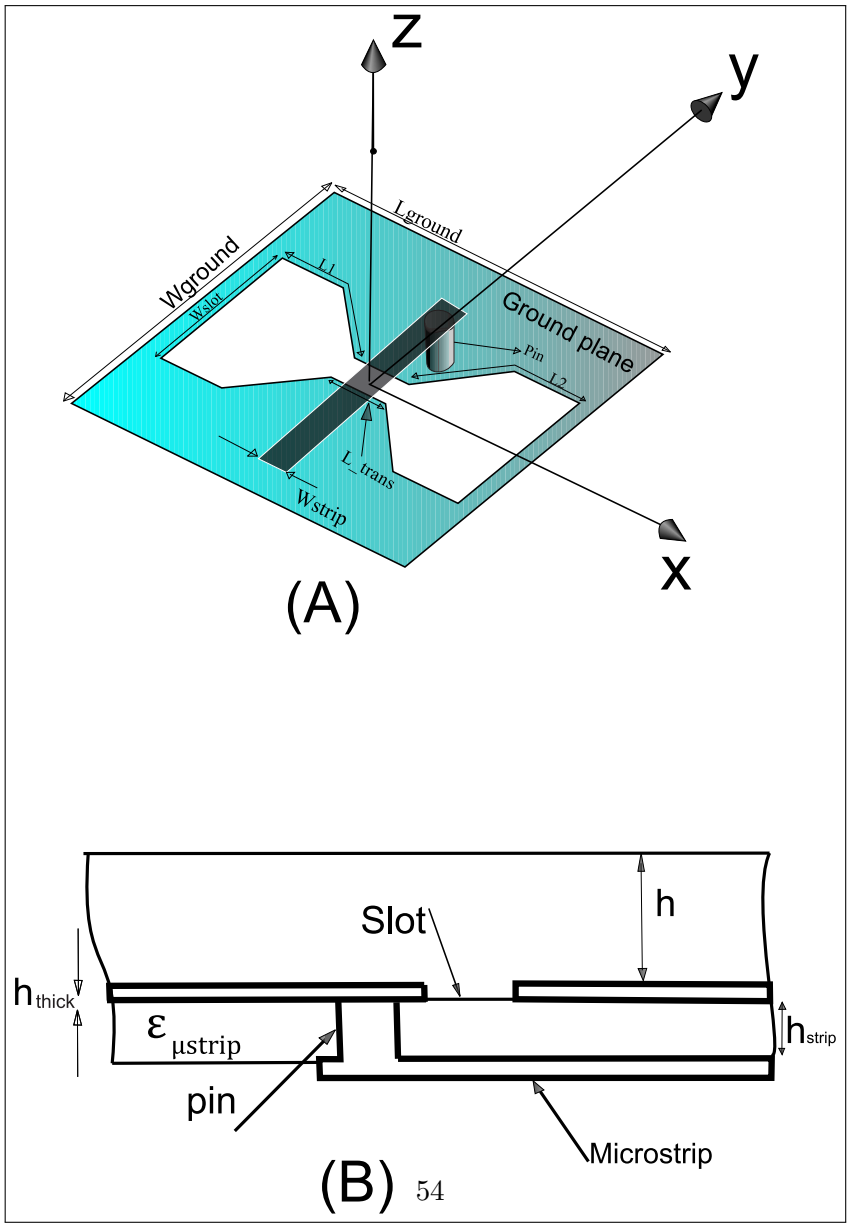

Figure 4.7: (A) Schematic sketch of new leaky slot antenna. (B) Cross sectional view of the new leaky slot antenna.

4.2.4 Reflection Coefficient and Simulation Process

The leaky slot antenna has been optimized to work effectively when the antenna is in contact with a matching medium of $\epsilon_r \approx 10.2$. The optimization process was done by using the commercial software CST microwave studio which is based on finite integration technique. The dimensions of the new antenna are summarized in Table 4.1

The simulated configuration is depicted in the Figure 4.9. For the sake of simplicity in the Figure 4.9 the feed configuration is not shown. However in the simulation analysis the feed configuration was included.

Our microwave imaging system utilizes dielectric constant (ϵ_r) 10.2 as ambient immersion medium, so 10.2 was assigned to the background of each simulation. However in the reality the leaky slot has 10.2 in one half of the space and ϵ_r =1 in the another half of the space which is depicted in Figure 4.9B. To perform this analysis in CST microwave studio, it is not possible to have infinite half space with one dielectric medium and infinite half space with another dielectric medium. So,10.2 was assigned to the background of each simulation and 50 mm thick block of air has been placed behind the slot which tries to mimic the true situation.

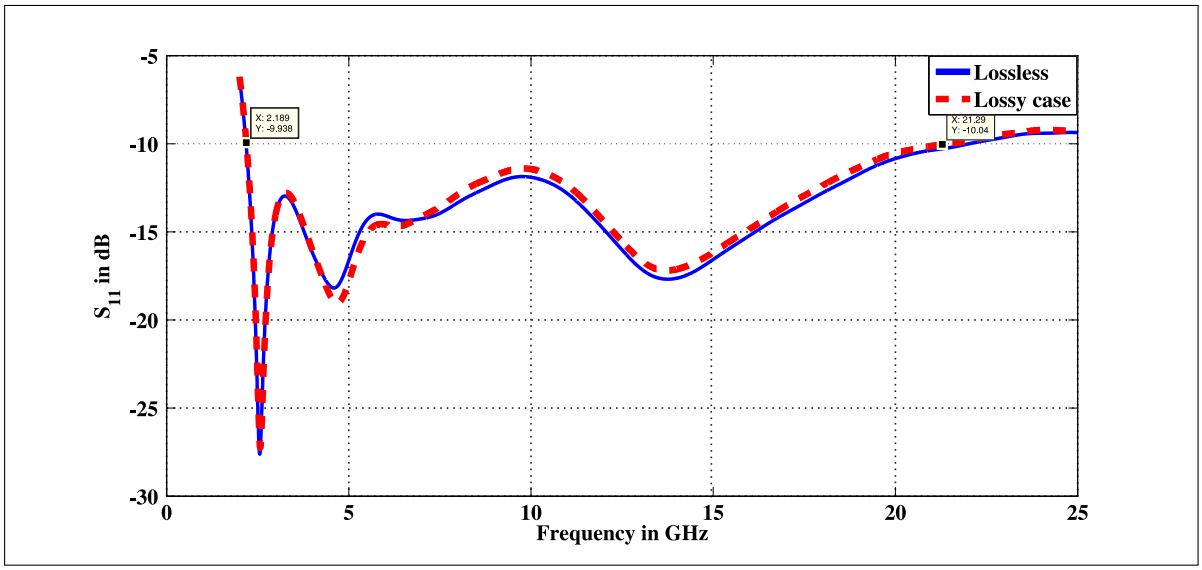

Figure 4.8: Reflection coefficient of LSPTFE in presence of lossless and lossy medium

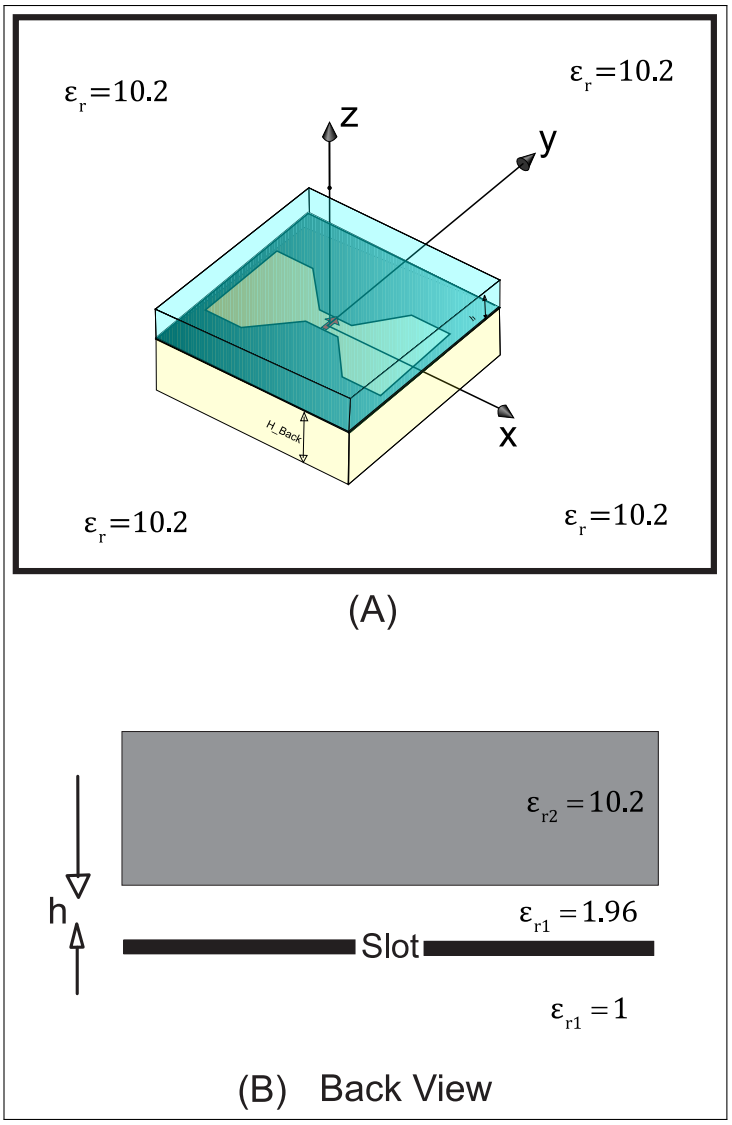

Figure 4.9: (A) Simulated leaky slot in 3D view where a block of airgap behind the slot can be observed. (B) Back view of the simulation set up

The matching for the antenna ($S_{11} \leq -10$ dB) has been obtained from 2 to 22 GHz (Figure 4.8), which gives almost 20 GHz of bandwidth to obtain fine resolution of images. The simulated S_{11} parameter has been normalized to 50 Ω. We can see both performances of the slot, in case of lossy and lossless medium condition. In case of lossy medium simulations the considered matching medium in the back ground simulations has a relative permittivity varying around 9 and 10 at frequencies between 2 and 10 GHz and attenuation of 2 dB/cm at a frequency of 8 GHz [35]. In both cases, the $S_{11} \leq -10$ dB in the required frequency range 3 -10 GHz.

4.2.5 Radiation Patterns of the Leaky Slot Antenna

The radiation patterns for the leaky slot antenna were calculated from 3 to 10 GHz and −3 dB beam width are reported over the bandwidth in Table 4.2. The principal planes cut

$\phi = 90°$ refers to the E plane which lies in y-z plane and the cut $\phi = 0°$ corresponds to the H plane which lies in x-z plane. The obtained radiation patterns are quite symmetrical in both principal planes and have wide beam width which satisfy the requirement of this application. The radiation patterns for the leaky slot antenna for both the principal planes can be seen in the Figure.4.10 and Figure.4.11. The 3D radiation pattern can be seen in the Figure.4.12 for 3 GHz frequency and Fig.4.13 is for 9 GHz frequency.

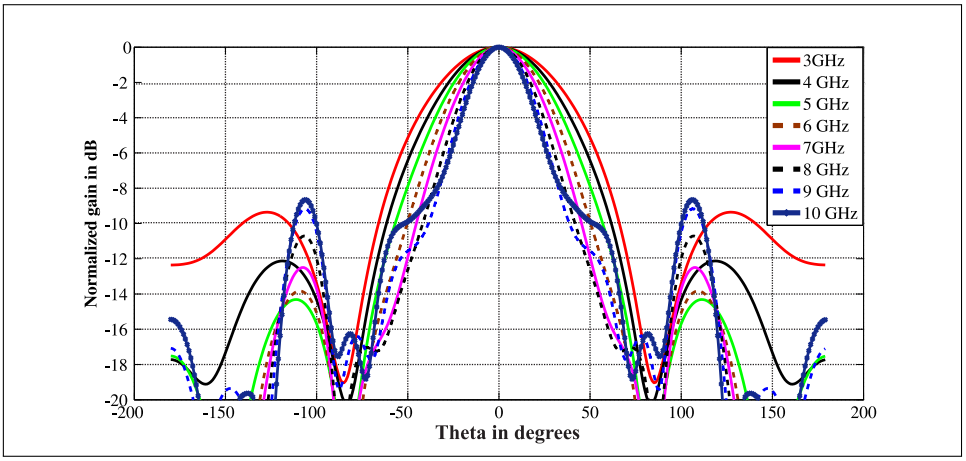

Figure 4.10: Radiation patterns in E plane

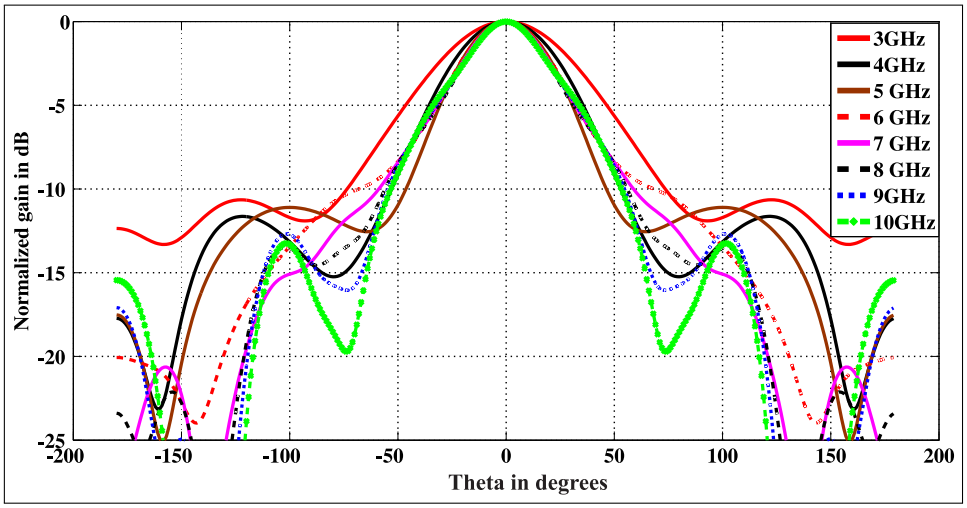

Figure 4.11: Radiation Patterns in H plane

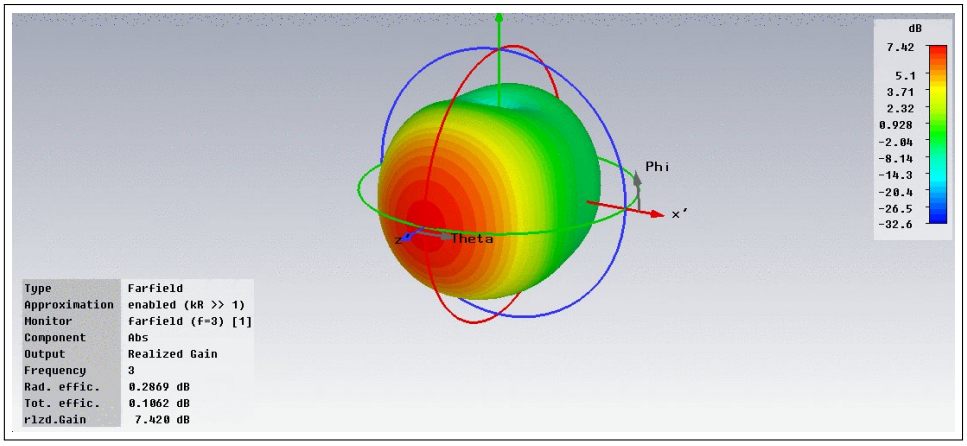

Figure 4.12: 3D Radiation pattern of LSPTFE at 3 GHz

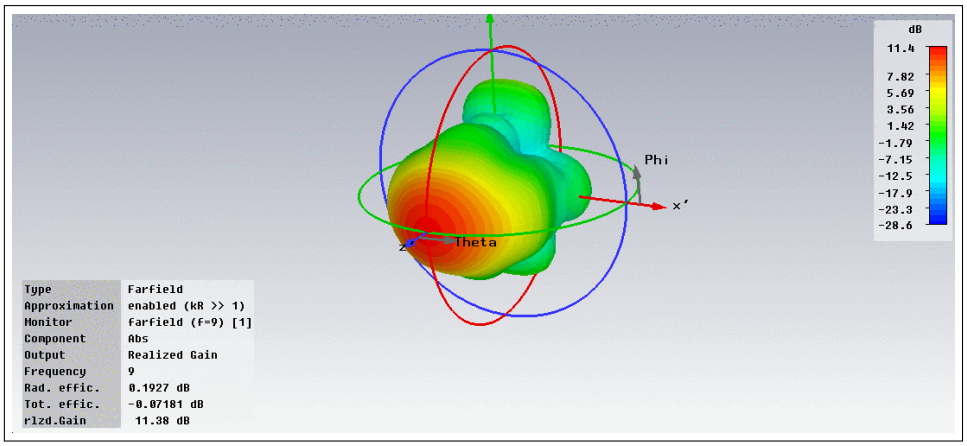

Figure 4.13: 3D Radiation pattern of LSPTFE at 9 GHz

Frequency in GHz	-3 dB Beamwidth (H-plane) deg	- 3dB Beamwidth (E-plane) deg
3	68.9	77.2
4	54.6	67.8
5	48.6	60.3
6	47.5	53.9
7	45.8	48.0
8	43.5	42.1
9	43.1	38.3
10	42.7	35.1

Table 4.2: Beam width of leaky slot antenna in principal planes

4.2.6 Gain and Front - to - Back ratio

The realized gain of leaky slot antenna is quite high and the simulated front to back ratio of this antenna is greater than -15 dB in the required frequency band region. The realized gain and overall efficiency are reported in Table 4.3. True front to back ratio cannot be computed in the simulations due to computational complexity, i.e infinite air layer behind the slot cannot be simulated.

However, Rutledge et al [41] earlier already showed that elementary dipole and slot antennas radiate most of their power into the dielectric with a factor of ϵ_r and $\epsilon_r^{\frac{3}{2}}$ respectively, over the power radiated into the air. For slot antennas the power in the dielectric completely dominates the power into the air, even at moderate dielectric constant. In our case the slot radiates into medium of dielectric constant ≈ 10.2. So from the above expressions for the slot the Front - to - back ratio would be better than -15 dB which confirms our simulation results.

Frequency in GHz	Realized gain in dB	Overall efficiency
3	7.424	1
4	8.695	0.97
5	9.625	1
6	9.9	1
7	10.68	1
8	11.18	0.98
9	11.38	0.98
10	11.52	0.9762

Table 4.3: Overall gain and efficiency of the leaky slot antenna

The simulated overall efficiency is greater than 0.97 in the required frequency range (Table. 4.3). Nevertheless, in the final realization of the demonstrator there could be additional ohmic losses in the strip line and mismatch losses at the connector during measurements which has to be accounted later.

4.2.7 Cross - Polar levels in Diagonal Planes

The cross polar levels are evaluated based on Ludwig 3 definition [21]. The co - polar and cross - polar gains on the diagonal plane for the leaky slot antenna are plotted for 3 GHz (Fig.4.14) and at 9 GHz frequency (Fig.4.15).

On an average $(\frac{F^{45^\circ}_{cross}}{F^{45^\circ}_{copolar}}) \geq -10$ dB in the whole required frequency range. The difference between the cross and co polar levels are plotted across the whole required frequency range in the Fig.4.16.

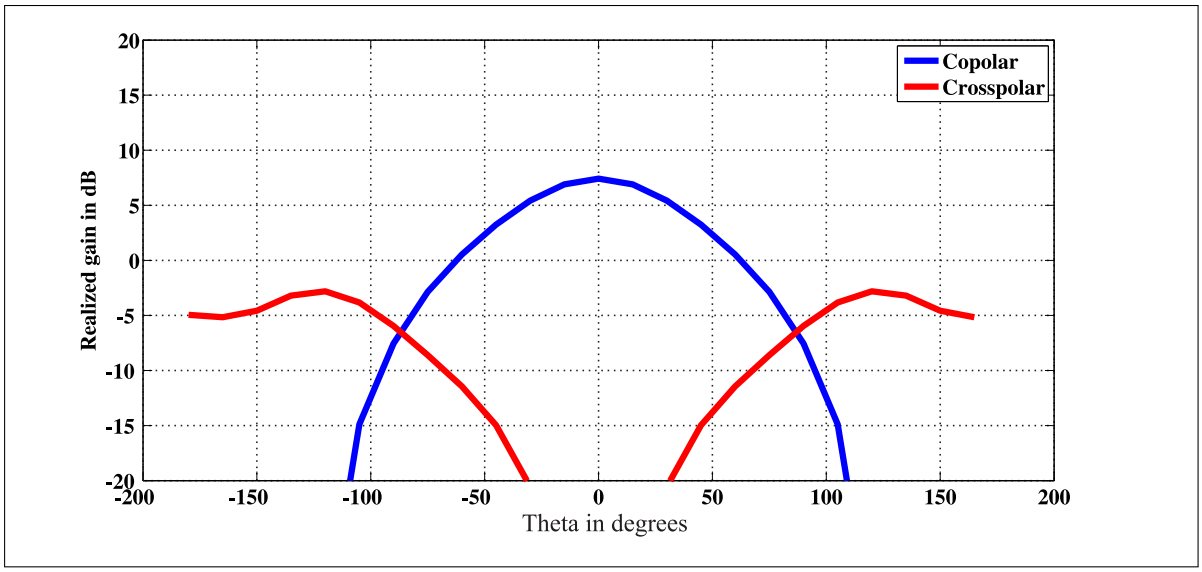

Figure 4.14: Cross Polar level at diagonal plane at 3 GHz

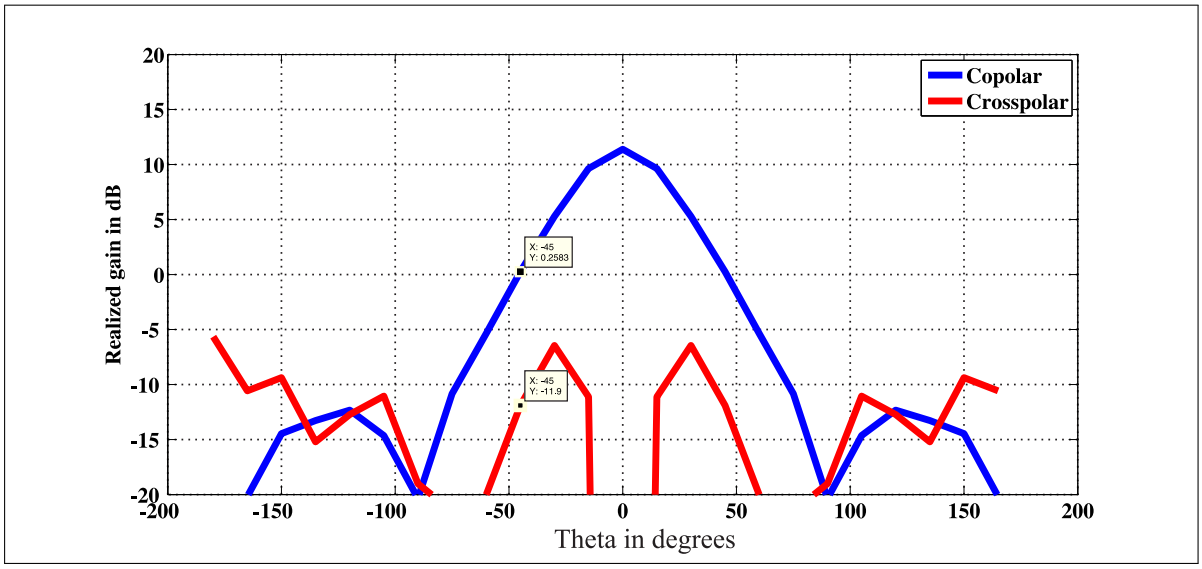

Figure 4.15: Cross Polar level at diagonal plane at 9 GHz

4.2.8 Transmission Response

In order to achieve a minimal distortion to the UWB signals transmitted inside the human body, the transfer function of the antenna has to be as flat as possible across the whole required range. From the results (Fig. 4.17) it can be seen that the S_{21} response is practically flat and lies well below -3 dB bandwidth across the required frequency range. In case of lossy condition the curve exhibits the slope because of the attenuation in the matching medium, which increases over the frequency as it was outlined in [35].

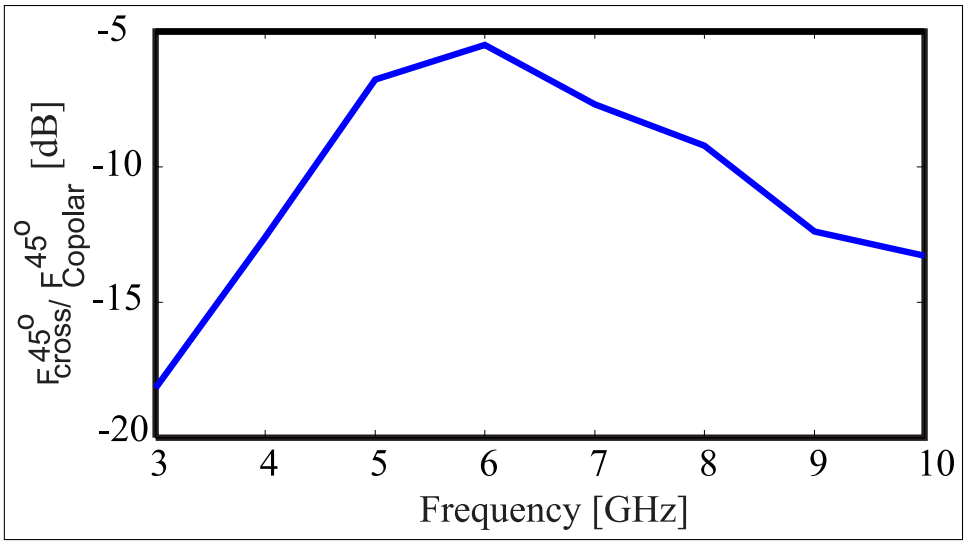

Figure 4.16: Cross Polar level at diagonal planes over the frequency region 3-10 GHz

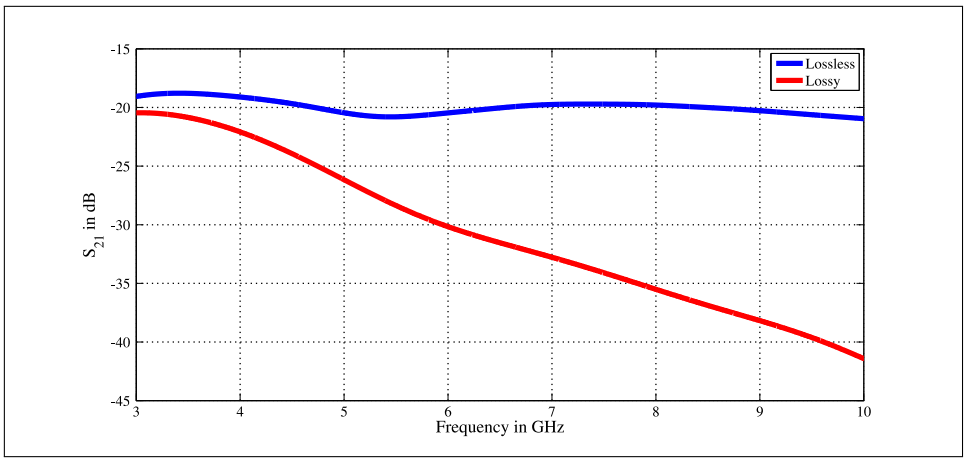

Figure 4.17: Transmission response of the leaky slot antenna in lossy and lossless case

The simulated S_{21} in lossy medium was calculated when the two antennas were facing each other through a block of the high dielectric medium (100 mm thick). In that block of high dielectric medium values with respective to relative permittivity varying around 9 and 10 at frequencies between 2 and 10 GHz and attenuation of 2 dB/cm at a frequency of 8 GHz [35] was incorporated.

4.2.9 Fidelity Factor Analysis

In order to study the level of the distortion of the radiated pulses, the fidelity factor analysis has been performed over the scanning region $\pm 60°$ in both the principal planes. As elucidated in chapter 2 the fidelity factor is the maximum magnitude of the cross correlation between the ideal signal response and simulated ideal response. According to this definition, fidelity factor was computed in both the principal planes. Figure 4.18 depicts the setup considered for evaluating FF in one of the principal planes.

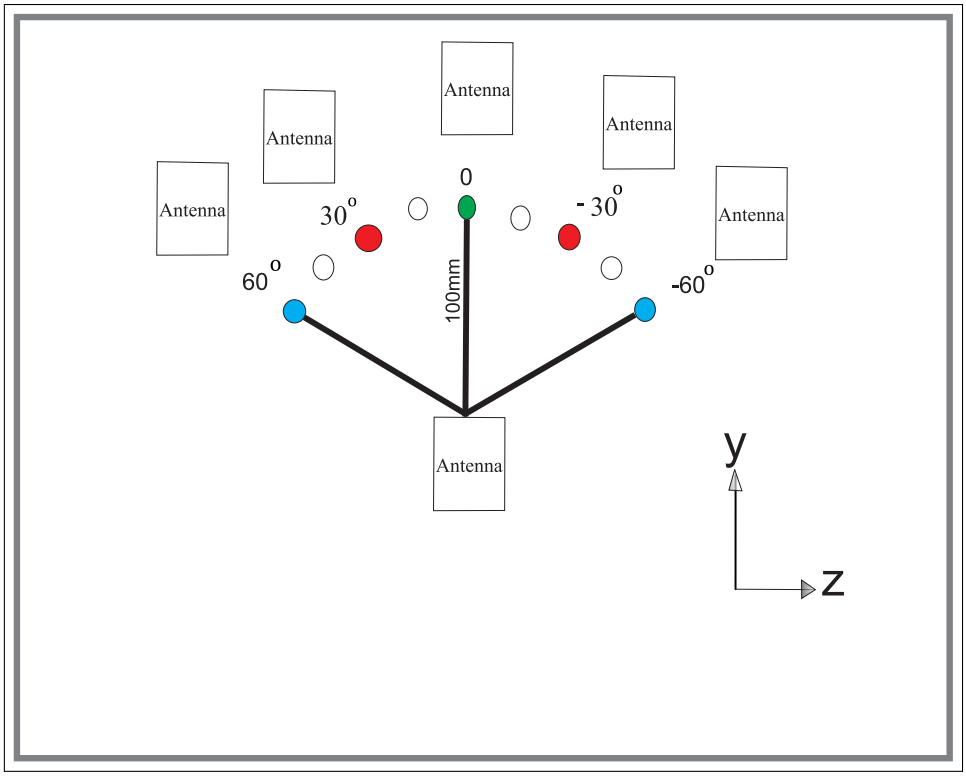

Figure 4.18: Schematic sketch for computing fidelity factor for ± 60° scanning range

4.2.10 Fidelity Factor Analysis of the Leaky- Slot Antenna in H plane, Principal cut - (x-z) Plane

For the entire simulated band (where $\omega_1 = 2\pi \times 3$GHz and $\omega_2 = 2\pi \times 10$ GHz) the Fidelity Factor (FF) of the link between two leaky slot antennas is calculated in H-plane for different angular ranges. In Figure 4.19 the fidelity factor of the link when the antenna is shifted to 15° from the bore sight direction is calculated and resulted to be 0.9857.

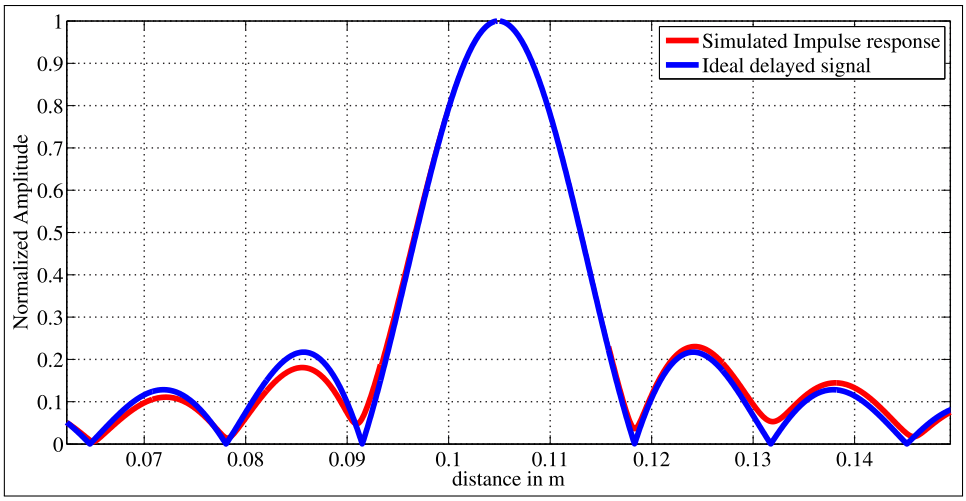

Figure 4.19: (3-10 GHz) pulse, antenna is shifted to 15° from the boresight direction in H Plane , fidelity = 0.9857

In Figure 4.20 the fidelity factor of the link when the antenna is shifted to 30° from the bore sight direction in H-plane is calculated and resulted to be 0.982.

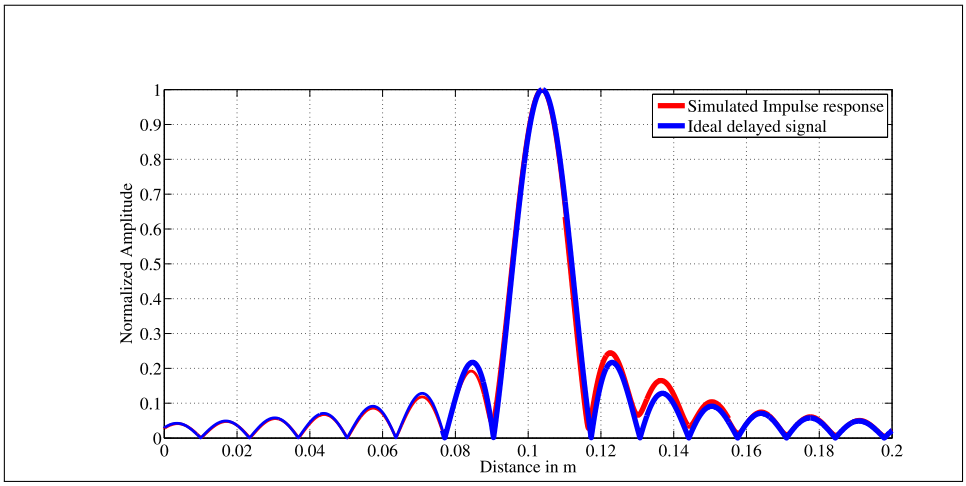

Figure 4.20: (3-10 GHz) pulse, antenna is shifted to 30° from the boresight direction in H Plane , Fidelity Factor = 0.982

In Figure 4.21 the fidelity factor of the link when the antenna is shifted to 45° from the bore sight direction in H-plane is calculated and resulted to be 0.98.

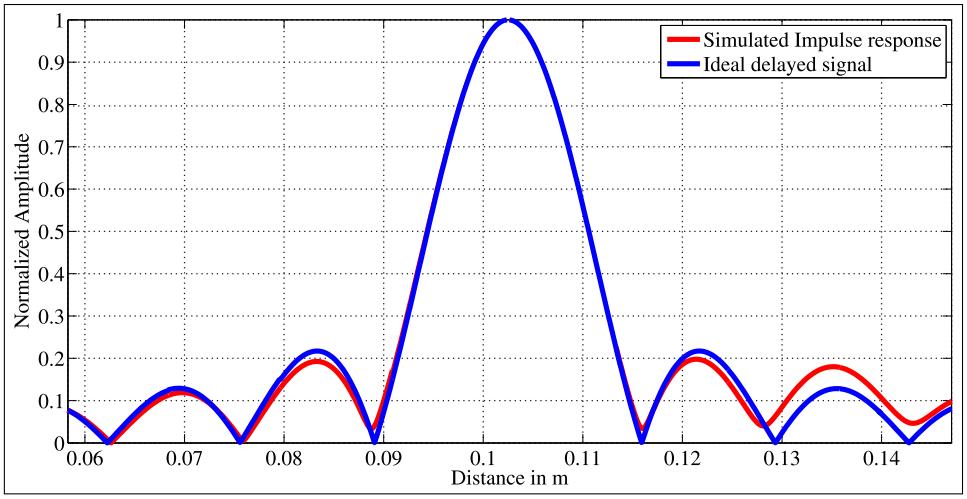

Figure 4.21: (3-10 GHz) pulse, antenna is shifted to 45° from the boresight direction in H Plane , Fidelity Factor = 0.98

To the best of my knowledge such a high fidelity factor on a frequency range 3-10 GHz has never been reported for radiated links for ± 60° scanning range.

4.2.11 Fidelity Factor Analysis of the Leaky- Slot antenna in E plane, Principal cut - (y-z) plane

Similarly FF analysis has been performed in E plane along ± 60° scanning range. The fidelity factor of the link when the antenna is shifted to 15° from the bore sight direction is calculated and depicted in Figure 4.22 which resulted to be 0.99.

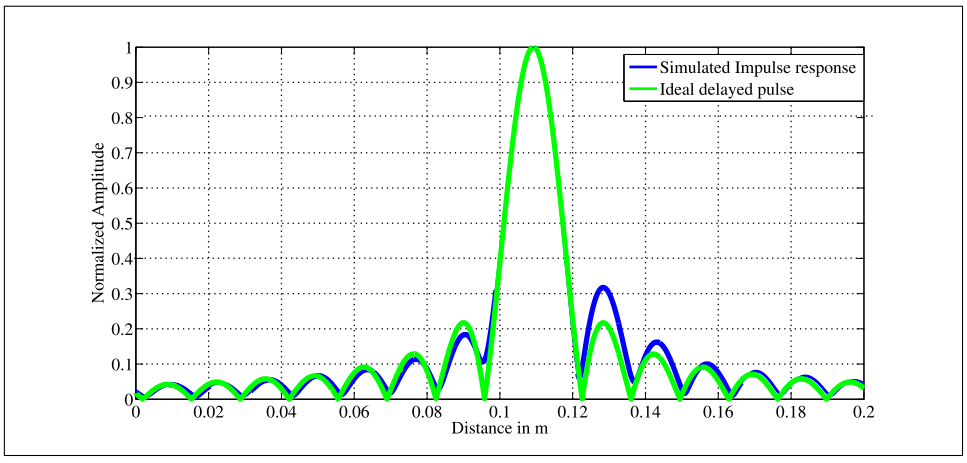

Figure 4.22: (3-10 GHz) pulse, antenna is shifted to 15° from the boresight direction in E Plane , Fidelity Factor = 0.99

In Figure 4.23 the fidelity factor of the link when the antenna is shifted to 30° from the bore sight direction in E-plane is calculated and resulted to be 0.97.

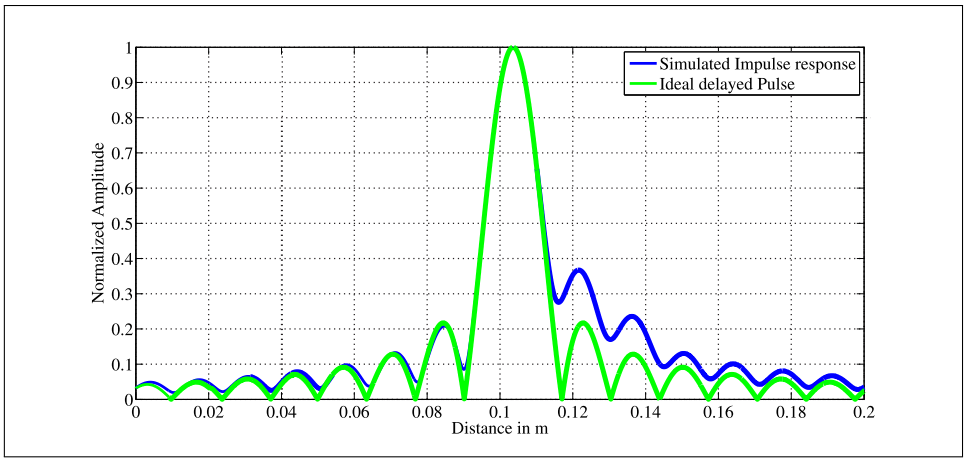

Figure 4.23: (3-10 GHz) pulse, antenna is shifted to 45° from the boresight direction in E Plane , Fidelity Factor = 0.97

In Figure 4.24 the fidelity factor of the link when the antenna is shifted to 60° from the bore sight direction in E-plane is calculated and resulted to be 0.96. The drop in FF value can be related back to the transfer function data (S_{21} in dB) at 60° and is most likely due to the rapid drop off seen in the signal content (i.e gain) at higher frequencies. However this only accounts a loss of 8% in the total transmitted power at 60° in E plane alone.

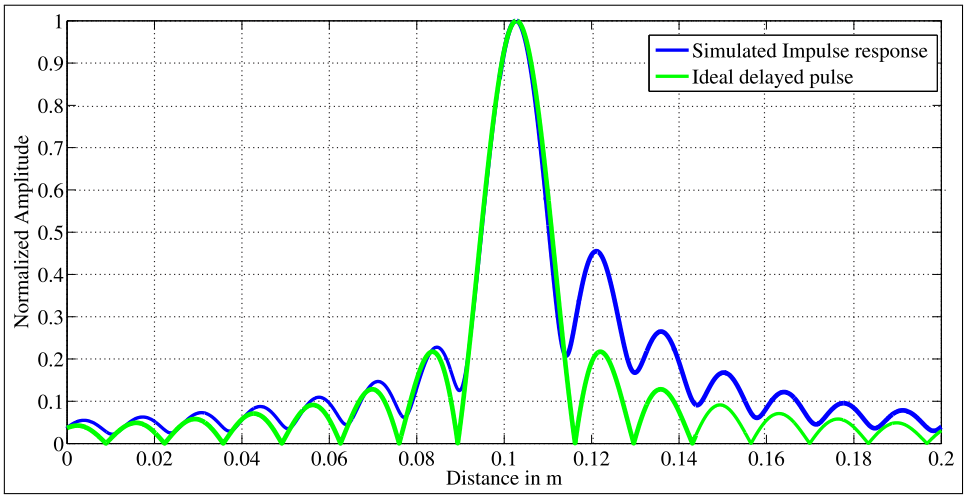

Figure 4.24: (3-10 GHz) pulse, antenna is shifted to 60° from the boresight direction in E Plane , Fidelity Factor= 0.96

In conclusion on the FF analysis for the leaky slot antenna is that it never drops FF value below 98% in principal H plane and never below 96% in principal E plane over the scanning region ± 60°.

4.2.12 Phase Center Calculations

4.2.12.1 Method -1

The phase center has been calculated for the leaky slot antenna in both the planes when the relative co-ordinate system is the same for the three frequencies 3, 5 and 8 GHz.

The procedure for calculating the phase center is elucidated as below :

The computed radiated far field versus θ, with reference to the 3 GHz co-ordinate system (x=0, y = 0,z = 0) has been considered for evaluating the phase center of the antenna. In this thesis application, we are interested to see the phase variations for - 3 dB beams in both the principal planes which are used for illuminating the interested region in the human body. Fig.4.25 and Fig.4.26 displays the simulated gains and phases of the radiation patterns for the new leaky slot antenna . Dotted lines mark the -3 dB beams. By fixing the reference system the phase center of the antenna has been calculated, it is evident that the phase of the slot in both principal planes are practically flat at 3 , 5 GHz and at 8 GHz frequency the variation of phase is 20° which is acceptable and does not induce much processing losses in the system.

4.2.12.2 Method -2

The excellent dispersivity properties that were presented in the fidelity factor analysis are due to both the linear growth of the gain and the linear variation of the phase of the received signal as a function of frequency. The gain can be derived from the amplitude of the $S_{12}(\omega)$, the phase variation over a certain frequency band can be read from the position of the peak of the link impulse response.

Fig.4.27 shows on the right scale the distance between the two antennas composing the link as derived from the position of the peak of the received signal in time domain over different frequency bands. Thus, for instance, performing the IFT of $S_{12}(\omega)$ by only retaining the frequency components from 3-6, 6-8, 8-10 GHz, one would observe that the peak of the received signal would arrive at a moment which corresponds to 113.45 , 115.2, 115.4 mm of propagation inside a dielectric medium of $\epsilon_r = 10.2$. Dividing this phase delay by two, one can observe that the corresponding variation of the phase center in each of the antennas is less than ± 0.4875 mm over the whole required frequency band.

This simulated demonstration about phase center only holds for the broad side links. On the basis of the results obtained with the two methods respectively, one can accept that the designed antenna can be stated as having a stable phase center.

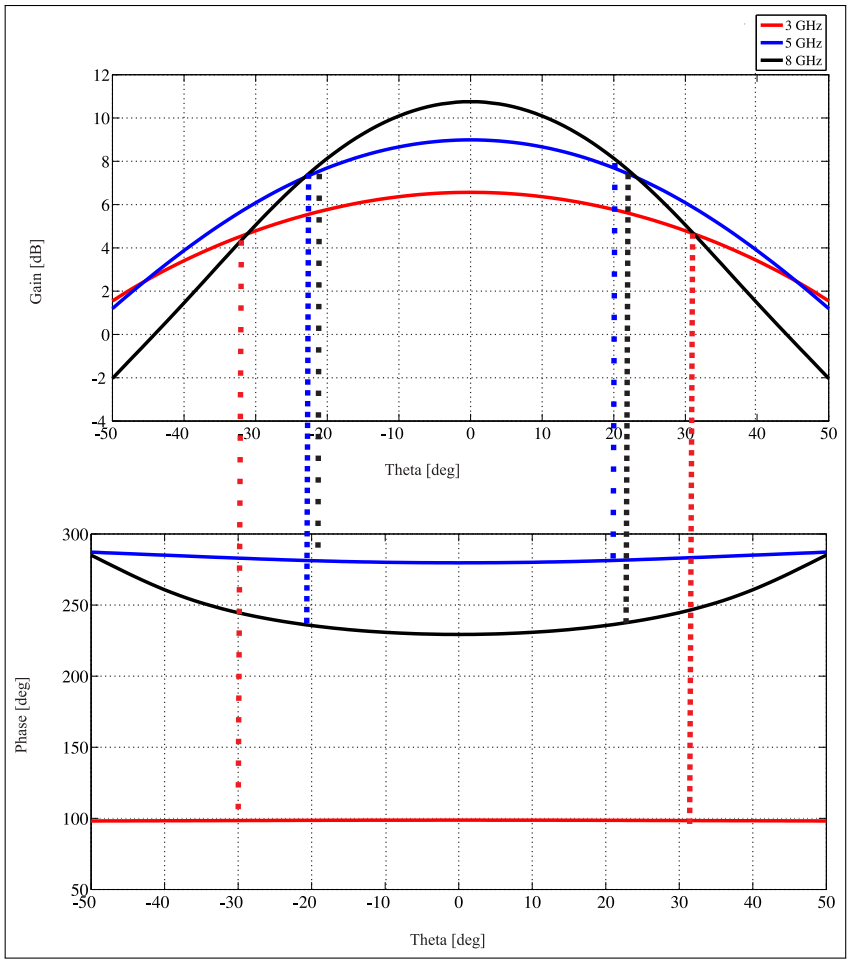

Figure 4.25: Radiation Pattern and Phase of new leaky slot antenna on E plane for analyzing -3 dB beamwidths. The relative co-ordinate system origin is the same for all three frequencies.

4.3 Conclusions:

The designed antenna can be summarized as following :

- S_{11} matching was obtained from 2 to 22 GHz giving ample amount of bandwidth to obtain fine resolution of images.
- The radiation patterns in both E and H planes are uniform in the required frequency range.
- The cross - polar levels in diagonal planes are low inside the dielectric medium.
- High fidelity performance in both the principal E and H planes is shown and no pulse distortion or ringing effect is observed in the simulations.
- High gain and efficiency which allows for a sufficient SNR such to penetrate deeper in human body tissues and for a high dynamic range of the radar is obtained.

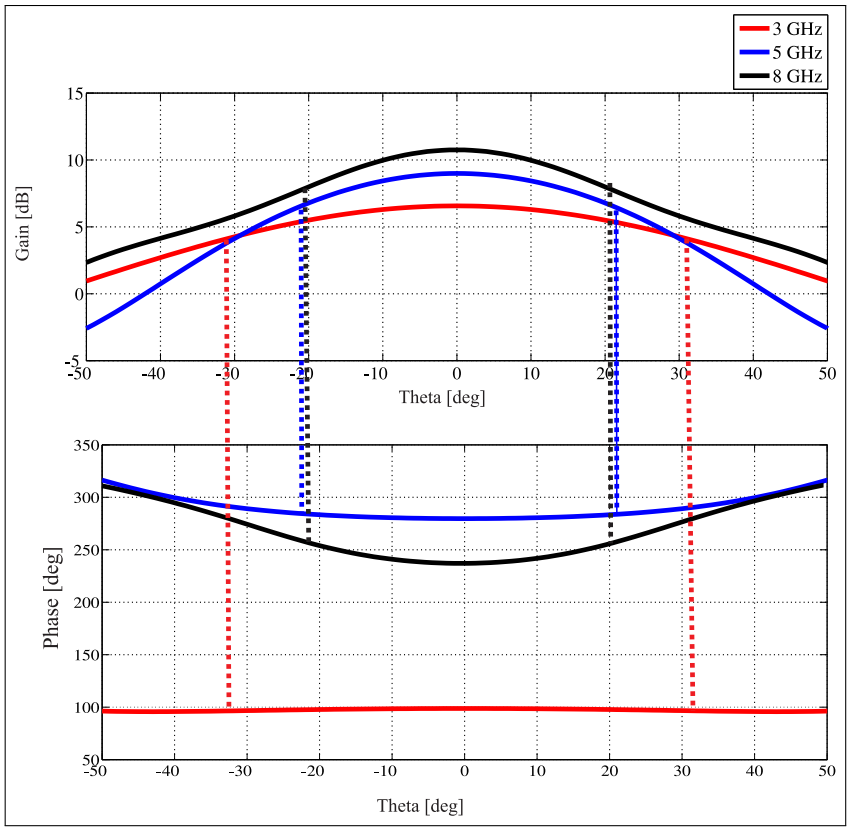

Figure 4.26: Radiation Pattern and Phase of new leaky slot antenna on H plane for analyzing −3 dB beamwidths. The relative co-ordinate system origin is the same for all three frequencies.

- The phase center of the antenna is practically flat for −3 dB beams which are of interest for this particular application.

With these properties the developed antenna could fit the requirements as a radiating element to be included in the radar system aimed at detecting tumors in the human body. Due to classification of the work, results with respect to Specific Absorption Rate (SAR) are not reported in this thesis. From the experimental analysis on SAR , it has been understood that majority of the radiated power is concentrated near the tumor due to the variation in high dielectric constant.

Further calculations of scattering from a multilayer phantom including a tumor, when the designed antenna is used in a MIMO array configuration have been carried out. Processing of the transmitter and the receiver signal demonstrated the capability of this system to detect even small tumors of size 5 mm. Due to the confidentiality issues, further details on this work cannot be published at this moment. Evaluation for this configuration and combination of tissue properties are still going on in TNO Netherlands.

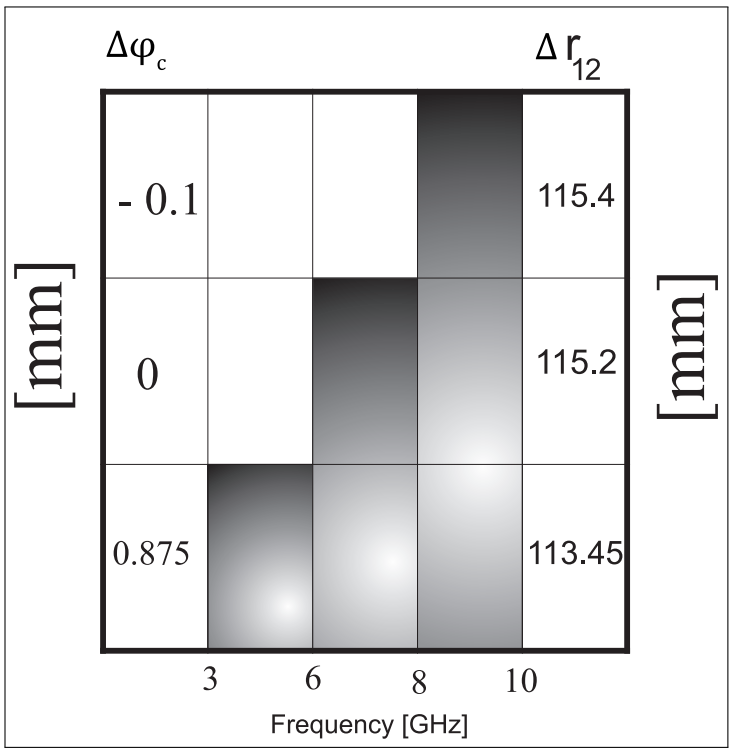

Figure 4.27: On the right scale : Optimal delay that should be introduced to recover 3 and 2 GHz BW pulses centered at different frequencies. On the left scale : Corresponding phase center variation with respect to the average.

Conclusions and Recommendations

5

In this chapter the conclusions of each chapter are summarized. This is followed by an overview of the scientific contributions made in this work. Subsequently, a list of recommendations is provided for future work.

5.1 Conclusions

Microwave imaging (MWI) is an attractive technique for imaging tumors in the human body. By designing an efficient antenna (leaky slot antenna) one can improve the quality of the radar system by enhancing the resolution of images. Today's biomedical diagnosis systems do not perform as needed because of the radiating element incorporated in the system which suffers in terms of efficiency, stable phase center and high gain. This was the reason to investigate and design a novel leaky slot antenna for UWB radar aimed at biomedical applications. This new antenna can offer good quality parameters for microwave imaging.

First a state of art research was carried out on the electrical characteristics of human tissues and understood the frequency dependency of the tissues. It was found that thickness of the skin layer varies with each patient and for the initial demonstration purpose it was decided to match the antenna to the medium of fatty tissue rather than to the skin which is consistent and has been the state of art till 2012.

The intrinsic limitations of the existing antennas in the open literature for the medical imaging has been discussed. Three UWB antennas are re-simulated to gain physical insight into their properties. It was understood from the simulations that microwave imaging setup built by University of Bristol has intrinsic limitations on the antenna design such as low efficiency, fidelity factor. Thus, an effective strategy has been applied to design a new novel leaky slot antenna which achieves the defined parameters for this particular application in chapter 2.

Extensive simulations were performed to design and analyze this new antenna. To the best of my knowledge and in comparison to the state of the art antennas, this is the only antenna which has high Fidelity Factor (FF) ($\geq 96\%$) over the scanning range $\pm 60^{\circ}$ in both the principal E and H planes.

Note that this antenna is the only one, to my knowledge which is at the same time efficient, weakly dispersive and with stable phase center. Low cross -polar levels inside the dielectric medium and efficiency higher than 90% make this a state of art antenna in tumor detection application.

Due to limited finances for this project , TNO could not manufacture and measure this antenna (leaky slot antenna developed in chapter 5).

In respect to the application analysis, the developed antenna appears to be suitable to detect objects buried inside the wet stand. However due to classification and to preserve the intellectual rights of TNO, the following results were not published or allowed to discuss in the thesis.

Also the results concerning the final system configuration and the processing of transmitter and receiver configuration results cannot be further discussed in respect to the application of tumor detection inside the human body. Simulations were carried out in circular and planar configurations which gave a input for designing a better image processing algorithm. In the end, a 5 mm tumor was successfully retrieved by using a bandwidth of only 5 GHz (3- 8 GHz) which gave confidence that this antenna could be a break through in the field of biomedical applications. For even better performances the antenna could be used in an array at low frequencies. Development of this array is being carried out in TU Delft at TeraHertz sensing group.

5.2 Recommendations

→ **Antenna design** :

Analytical expressions of the radiated fields for the developed leaky slot antenna could be calculated in future. This expressions could help to understand the behavior of the antenna and help to exactly quantify why the cross polarization is quite low in diagonal planes in comparison with earlier leaky slot antenna developed for exciting the lens and speed up the design procedure.

The results presented in this work are based on the simulations of leaky slot antenna developed in chapter 5. If the antenna is manufactured and measured, it would be interesting to know the mechanical tolerances and discrepancies caused either by connector or due to variation in the matching medium of the liquid considered for measurement purposes.

The designed antenna exhibits linear polarization, however the tumor backscatters in both polarizations (Co and Cross polar). In order to capture both polarizations of the back scattered signal, in future an antenna with circularly polarization would be better for imaging purpose.

→ **SAR Computations** :

One could get human body voxel provided by commerical software solvers like CST rather than manually incorporating the dielectric values into the multilayered phantom. This could yield accurate results for SAR calculations and less compuational work.

5.3 Publications in respect to my thesis:

→ A leaky wave antenna for radar medical imaging by K. Vaddagiri, S. Monni , A. Neto in 2012 IEEE International Symposium on Antennas and Propagation and USNC-URSI National Radio Science Meeting Chicago 2012 July 8-13. (Published).

Bibliography

[1] Colleen J. Fox, Paul M. Meaney, Fridon Shubitidze, Lincoln Potwin, and Keith D. Paulsen. Characterization of an implicitly resistively-loaded monopole antenna in lossy liquid media. *International Journal of Antennas and Propagation*, -:1 –4, 2008.

[2] D. Gibbins, M. Klemm, I.J. Craddock, J.A. Leendertz, A. Preece, and R. Benjamin. A comparison of a wide-slot and a stacked patch antenna for the purpose of breast cancer detection. *Antennas and Propagation, IEEE Transactions on*, 58(3):665 –674, Mar. 2010.

[3] A.Neto. Uwb, non dispersive radiation from the planarly fed leaky lens antenna ; part 1 : Theory and design. *Antennas and Propagation, IEEE Transactions on*, 58(7):2238 –2247, July 2010.

[4] Federal Communications Commission Commission. Revision of part 15 of the commission's rules, August,14 2006.

[5] Electronic Communications Committee Committee. Ecc decision on the harmonised conditions for devices using ultra-wideband (uwb) technology in bands below 10.6 ghz., March,24 2006.

[6] Unapproved revised pc95.1b (draft ieee standard for safety levels with respect to human exposure to radio frequency electromagnetic fields, 3 khz to 300 ghz amendment 1: Specific absorption rate (sar) limits for the pinna) (amendment 1 to ieee std c95.1-1991 (1999 ed.) c95.1b) superseded by c95.1/d2.4, 2005.

[7] L. E. Larsen and J. H. Jacobi. The use of orthogonal polarizations in microwave imagery of isolated canine kidney. *Nuclear Science, IEEE Transactions on*, 27(3):1183 –1191, Jun. 1980.

[8] Netherlands Central Bureau of Statistics. Cancer mortality by type of cancer. Statistics Netherlands, 2010.

[9] Global cancer facts & figures 2nd edition, 2011.

[10] E.K.Fry, Kossoff.K, and H.Hindman. The potential of ultrasound visualization for detecting the presence of abnormal structures within the female breast. In *1972 Ultrasonics Symposium*, pages 25 – 30, 1972.

[11] A.Banerjee and R.Chellappa. Tumor detection in digital mammograms. In *Image Processing, 2000. Proceedings. 2000 International Conference on*, volume 3, pages 432 –435 vol.3, 2000.

[12] P. T. Huynh, A. M. Jarolimek, and S. Daye. The false-negative mammogram. *Radiographics*, 18:1137 1154,, 1998.

[13] Olivier Zachariae, Friedemann Baum, Dorit von Heyden, Matthias Funke, and Torsten Liersch. The influence of preoperative mri of the breasts on recurrence rate in patients with breast cancer. *European Radiology*, 14:1725–1731, 2004.

[14] S. S. Chaudhary, R. K. Mishra, A. Swarup, and J. M. Thomas. Dielectric properties of normal and malignant human breast tissues at radiowave and microwave frequencies. *Indian J. Biochem. and Biophys.,*, 21:76–79, Feb 1984.

[15] W. T. Joines, Y. Z. Dhenxing, and R. L. Jirtle. The measured electrical properties of normal and malignant human tissues from 50 to 900 mhz. *Med. Phys*, 21:547–550, Apr. 1994.

[16] Xu Li, E.J. Bond, B.D. Van Veen, and S.C. Hagness. An overview of ultra-wideband microwave imaging via space-time beamforming for early-stage breast-cancer detection. *Antennas and Propagation Magazine, IEEE*, 47(1):19 – 34, feb 2005.

[17] D. Gibbins, M. Klemm, J. A. Leendertz, A. Preece, and R. Benjamin. Clinical trials of a uwb imaging radar for breast cancer. *Antennas and Propagation (EuCAP), 2010 Proceedings of the Fourth European Conference on*, 0(3):1–4, Mar. 2010.

[18] D. J. Kurrant, E. C. Fear, and D. T. Westwick. Tumor estimation in tissue sensing adaptive radar (tsar) signals. *Electrical and Computer Engineering, 2007. CCECE 2007.*, 0:860–863, April 2007.

[19] F. Sabath, E. L. Mokole, and S. N. Samaddar. Definition and classication of ultra-wideband signals and devices. *Radio Science*, 1(313):12–26, June 2005.

[20] C. A. Balanis. Antenna theory, analysis and design, 2nd edition,, 1982.

[21] A. Ludwig. The definition of cross polarization. *Antennas and Propagation, IEEE Transactions on*, 21(1):116 – 119, Jan 1973.

[22] IEEE. Ieee standard definitions of terms for antennas, 1983.

[23] D. Cavallo. An investigation on the performance of ultra-wide-band (uwb) tapered slot antennas and arrays. Master's thesis, , Dept. Engineering, University of Sannio, Benevento, Italy, 2007.

[24] W. Sorgel and W. Wiesbeck. Influence of the antennas on the ultra- wideband transmission. *EURASIP Journal on Applied Signal Processing*, no.3:pp. 296–305, 2005.

[25] A. Mehdipour, K. Mohammadpour-Aghdam, and R. Faraji-Dana. Complete dispersion analysis of vivaldi antenna for ultra wideband applications. *Progress In Electromagnetics Research*, 77:85–96, 2007.

[26] T.P Montoya and G.S. Smith. A study of pulse radiation from several broad-band loaded monopoles. *Antennas and Propagation, IEEE Transactions on*, 44(8):1172 –1182, aug 1996.

[27] E.M. Staderini. Uwb radars in medicine. *Aerospace and Electronic Systems Magazine, IEEE*, 17(1):13 –18, jan 2002.

[28] D. Gibbins, M. Klemm, I. J. Craddock, J. A. Leendertz, A. Preece, and R. Benjamin. Experimental and clinical results of breast cancer detection using uwb microwave radar. In *Antennas and Propagation Society International Symposium, 2008. AP-S 2008. IEEE*, pages 1 –4, July. 2008.

[29] A.A.Lestari, E. Bharata, A. B. Suksmono, A. Kurniawan, A. G. Yarovoy, and L. P. Ligthart. A modified bow-tie antenna for improved pulse radiation. *Antennas and Propagation, IEEE Transactions on*, 58(7):2184 –2192, July 2010.

[30] Xu Li, S. C. Hagness, M. K. Choi, and D.W. Van der Weide. Numerical and experimental investigation of an ultrawideband ridged pyramidal horn antenna with curved launching plane for pulse radiation. *Antennas and Wireless Propagation Letters, IEEE*, 2(1):259 –262, 2003.

[31] H.Xin H.Zhang and R.W. Ziolkowski. Design of novel printed elliptical monopole antenna for uwb applications. In *Antennas and Propagation Society International Symposium, 2008. AP-S 2008. IEEE*, pages 1 –4, July 2008.

[32] Q.Ye and Zhi Ning Chen. A novel butterfly-shaped monopole uwb antenna. In *Antenna Technology: Small and Smart Antennas Metamaterials and Applications, 2007. IWAT '07. International Workshop on*, pages 315 –318, march 2007.

[33] Liang, Jianxin, Chiau, X.Chen, and C. G. Parini. Study of a printed circular disc monopole antenna for uwb systems. *Antennas and Propagation, IEEE Transactions on*, 53(11):3500 – 3504, Nov. 2005.

[34] B.S.Yildirim, B.A.Cetiner, G. Roqueta, and L. Jofre. Integrated bluetooth and uwb antenna. *Antennas and Wireless Propagation Letters, IEEE*, 8:149 –152, 2009.

[35] D. Gibbins, M. Klemm, I. J. Craddock, J. A. Leendertz, A. Preece, and R. Benjamin. Microwave radar-based breast cancer detection: Imaging in inhomogeneous breast phantoms. *Antennas and Wireless Propagation Letters, IEEE*, 8:1349 –1352, 2009.

[36] A.Neto and S.Maci. Green's function for an infinite slot printed between two homogeneous dielectrics. i. magnetic currents. *Antennas and Propagation, IEEE Transactions on*, 51(7):1572 – 1581, July 2003.

[37] S.Maci and A. Neto. Green's function of an infinite slot printed between two homogeneous dielectrics-part ii: uniform asymptotic solution. *Antennas and Propagation, IEEE Transactions on*, 52(3):666 – 676, Mar. 2004.

[38] S S.Bruni, A. Neto, and F. Marliani. The ultrawideband leaky lens antenna. *Antennas and Propagation, IEEE Transactions on*, 55(10):2642 –2653, oct. 2007.

[39] A. Neto, S. Monni, and F. Nennie. "uwb, non dispersive radiation from the planarly fed leaky lens antennapart ii: Demonstrators and measurements". *Antennas and Propagation, IEEE Transactions on*, vol.58:pp.2248–2258, July 2010.

[40] Cst microwave studio, cst, germany, user manual 8.0 version, 2008. Darmstadt, Germany.

[41] D.Rutledge and M. Muha. Imaging antenna arrays. *Antennas and Propagation, IEEE Transactions on*, 30(4):535 – 540, July 1982.